https://doi.org/10.5194/egusphere-2025-4069
Preprint. Discussion started: 14 October 2025

Disentangling uncertainty in ISMIP6 Antarctic sub-shelf melting and 2300 sea level rise projections

Johanna Beckmann[1], Ronja Reese[2], Felicity S. McCormack[1], Sue Cook[3], Lawrence Bird[1], David Gwyther[4], Daniel Richards[5,6], Matthias Scheiter[5], Yu Wang[3], Hélène Seroussi[7], Ayako Abe-Ouchi[8], Torsten Albrecht[9,10], Jorge Alvarez-Solas[11,12], Xylar S. Asay-Davis[13], Jean-Baptiste Barre[14], Constantijn J. Berends[15], Jorge Bernales[15], Javier Blasco[16], Justine Caillet[17,7], David M. Chandler[18], Violaine Coulon[19], Richard Cullather[20], Christophe Dumas[21], Benjamin K. Galton-Fenzi[3,22], Julius Garbe[9,23], Fabien Gillet-Chaulet[17], Rupert Gladstone[24], Heiko Goelzer[18], Nicholas R. Golledge[25], Ralf Greve[26,27], G. Hilmar Gudmundsson[2], Holly Kyeore Han[13,28], Trevor R. Hillebrand[13], Matthew J. Hoffman[13], Philippe Huybrechts[29], Nicolas C. Jourdain[17], Ann Kristin Klose[9,23], Petra M. Langebroek[18], Gunter R. Leguy[30], William H. Lipscomb[30], Daniel P. Lowry[31], Pierre Mathiot[17], Marisa Montoya[11,12], Mathieu Morlighem[32], Sophie Nowicki[33], Frank Pattyn[19], Antony J. Payne[34], Tyler Pelle[35], Aurélien Quiquet[21], Alexander Robinson[11,16], Leopekka Saraste[36], Erika G. Simon[20], Sainan Sun[2], Jake P. Twarog[7], Luke D. Trusel[37], Benoit Urruty[17], Jonas Van Breedam[29], Roderik S. W. van de Wal[15,38,39], Chen Zhao[3], and Thomas Zwinger[36]

[1]Securing Antarctica's Environmental Future, School of Earth, Atmosphere & Environment, Monash University, Clayton, Kulin Nations, Victoria, Australia
[2]Northumbria University, Newcastle, UK
[3]Australian Antarctic Program Partnership, Institute for Marine and Antarctic Studies, University of Tasmania, Nipaluna / Hobart, Lutruwita / Tasmania, Australia
[4]School of Earth and Environmental Sciences, The University of Queensland, St Lucia, Queensland, Australia
[5]Australian Centre for Excellence in Antarctic Science, Institute for Marine and Antarctic Studies, University of Tasmania, Nipaluna / Hobart, Lutruwita / Tasmania, Australia
[6]British Antarctic Survey, Cambridge, England, UK
[7]Thayer School of Engineering, Dartmouth College, Hanover, NH, USA
[8]Atmosphere and Ocean Research Institute, University of Tokyo, Kashiwa, Japan
[9]Potsdam Institute for Climate Impact Research (PIK), Member of the Leibniz Association, Potsdam, Germany
[10] Department of Integrative Earth System Science, Max Planck Institute of Geoanthropology, Kahlaische Str. 10, 07745 Jena, Germany
[11]Departamento de Física de la Tierra y Astrofísica, Facultad de Ciencias Físicas, Universidad Complutense de Madrid, Madrid, Spain
[12]Instituto de Geociencias, Consejo Superior de Investigaciones Científicas, Universidad Complutense de Madrid, Madrid, Spain
[13]Fluid Dynamics and Solid Mechanics Group, Los Alamos National Laboratory, Los Alamos, NM, USA
[14]Department of Earth System Science, University of California Irvine, Irvine, CA, USA
[15]Institute for Marine and Atmospheric Research Utrecht, Utrecht University, Utrecht, The Netherlands
[16]Alfred Wegener Institute, Helmholtz Centre for Polar and Marine Research, Potsdam, Germany
[17]Univ. Grenoble Alpes/CNRS/INRAE/IRD/G-INP, Institut des Géosciences de l'Environnement, Grenoble, France
[18]NORCE Norwegian Research Centre, Bjerknes Centre for Climate Research, Bergen, Norway
[19]Laboratoire de Glaciologie, Université libre de Bruxelles, Brussels, Belgium
[20]NASA Goddard Space Flight Center, Greenbelt, MD, USA

https://doi.org/10.5194/egusphere-2025-4069
Preprint. Discussion started: 14 October 2025

[21]Laboratoire des Sciences du Climat et de l'environnement, LSCE-IPSL, CEA-CNRS-UVSQ, Université Paris-Saclay, Paris, France
[22]Australian Antarctic Division, Kingston, Tasmania, Australia
[23]Institute of Physics and Astronomy, University of Potsdam, Potsdam, Germany
[24]Arctic Centre, University of Lapland, Rovaniemi, Finland
[25]Antarctic Research Centre, Victoria University of Wellington, Wellington, New Zealand
[26]Institute of Low Temperature Science, Hokkaido University, Sapporo, Japan
[27]Arctic Research Center, Hokkaido University, Sapporo, Japan
[28]Earth Surface and Interior Group, Jet Propulsion Laboratory, Pasadena, CA, USA
[29]Earth System Science & Departement Geografie, Vrije Universiteit Brussel, Brussels, Belgium
[30]Climate and Global Dynamics Laboratory, NSF National Center for Atmospheric Research, Boulder, CO, USA
[31]GNS Science, Lower Hutt, New Zealand
[32]Department of Earth Sciences, Dartmouth College, Hanover, NH, USA
[33]Department of Geology, University at Buffalo, Buffalo, NY, USA
[34]University of Liverpool, Liverpool, UK
[35]Scripps Institution of Oceanography, University of California San Diego, La Jolla, CA, USA
[36]CSC-IT Center for Science, Espoo, Finland
[37]Department of Geography, Pennsylvania State University, University Park, PA, USA
[38]Department of Physical Geography, Utrecht University, Utrecht, The Netherlands
[39]The Royal Netherlands Meteorological Institute, De Bilt, The Netherlands

Correspondence: Johanna Beckmann (johanna.beckmann@monash.edu)

Abstract. Ocean-driven ice shelf melting is a major contributor of present and future ice loss from the Antarctic Ice Sheet. In the Ice Sheet Model Intercomparison Project (ISMIP6) Antarctic 2300 projections, sea level rise varies widely, from -0.6 to 4.4 m, highlighting significant uncertainty. Here, we assess drivers of this spread, focussing on sub-shelf melting and dynamic ice loss as well as sectors that have the potential for large-scale, rapid ice loss: the Amundsen Sea, Filchner-Ronne, and Ross sectors, and the Aurora and Wilkes Subglacial Basins. We derive two sensitivity factors for each ISMIP6 simulation: a) a melt sensitivity factor, describing how simulated sub-shelf melt rates respond to ocean thermal forcing changes; and b) a dynamic ice loss sensitivity factor, describing how simulated dynamic ice loss (and hence sea level contribution) responds to cumulative sub-shelf melt changes. Melt sensitivities range from 1.5–21.3 $\mathrm{ma}^{-1}\mathrm{K}^{-1}$, with no clear dependency on the melt parameterisation. Model simulations cluster into two groups based on calving strength. The dynamic ice loss sensitivities range from 0.1 to 2.6 (unitless), with larger variations in the Amundsen sector, and Aurora and Wilkes Subglacial Basins. These sensitivity factors are good predictors of short-term integrated melting and sea level rise, respectively, but are less robust on longer time scales. Our findings show that these factors explain much of the ensemble spread in projected ice loss to 2300. We recommend to further constrain these factors, and advocate for their use in model calibration and emulator design, with the ultimate aim of explaining uncertainties in future projections of sea level rise from Antarctica.

1 Introduction

Future ice loss from the Antarctic Ice Sheet constitutes the largest source of uncertainty in projections of sea level rise under various greenhouse gas emission scenarios (Fox-Kemper et al., 2021). Melting beneath the ice shelves that surround the Antarctic

https://doi.org/10.5194/egusphere-2025-4069
Preprint. Discussion started: 14 October 2025

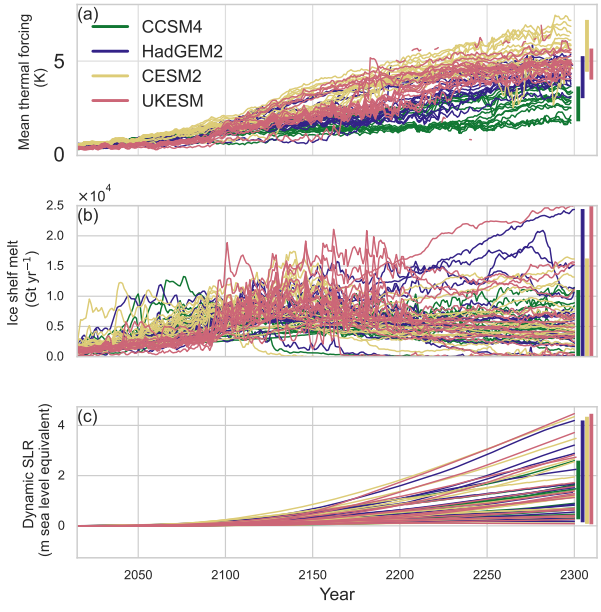

Figure 1. ISMIP6 Antarctic 2015-2300 projections of (a) Antarctic-wide ocean thermal forcing averaged over water masses right underneath ice shelves (K); (b) total ice shelf basal mass balance ($\mathrm{Gt\,yr^{-1}}$); and (c) cumulative dynamic sea level rise (SLR; m sea level equivalent). Each line corresponds to an ice sheet model simulation, and results are coloured by the climate model forcing experiment for the high-emission scenarios, namely: CCSM4 (green; exp02); HadGEM2 (blue; exp03); CESM2 (yellow; exp04); and UKESM (pink; exp05).

continent will be a key driver of ice loss in the coming decades to centuries (Seroussi et al., 2020, 2023, 2024). However, there are a number of open questions surrounding sub-shelf melt processes (e.g., Fricker et al., 2025) and how their implementation in numerical simulations contributes to the broad spread in future Antarctic mass budget trajectories. Projections of Antarctic ice loss to 2100 from the Ice Sheet Model Intercomparison Project for CMIP6 (ISMIP6; Nowicki et al., 2020) range from slight mass gains (equivalent to 0.078 m of sea level lowering) to ice losses equivalent to more than 0.3 m of sea level rise for high emission scenarios (RCP8.5 or SSP5-8.5; Seroussi et al., 2020). High-end projections from the Linear Antarctic Response to basal melting Model Intercomparison Project 2 (LARMIP2; Levermann et al., 2020) are even higher, with a very likely range between 0.06 and 0.58 m, although these projections exclude changes in surface accumulation. More recent ISMIP6 results extended to 2300 (ISMIP6 2300; Seroussi et al., 2024) show that Antarctica could contribute between -0.6 and 4.4 m by 2300 under unabated climate change. The largest sources of variance in the ISMIP6 2100 Antarctic projections of dynamic ice loss, focusing on the dynamic response to oceanic changes and based on constant surface mass balance forcing, come from choices made in the ice sheet models and ice-climate interactions, including the representation of sub-shelf melting (Seroussi et al., 2023). This is illustrated also in Fig. 1, which represents results from the ISMIP6 2300 Antarctic projections Seroussi et al. (2024) and is the primary motivation for our study: while variations in projected ocean thermal forcing can be clearly linked to the corresponding climate models for the simulations in ISMIP6 Antarctic 2300 (Fig. 1a), the corresponding simulated basal

https://doi.org/10.5194/egusphere-2025-4069
Preprint. Discussion started: 14 October 2025

mass balance (Fig. 1b) and dynamic ice loss (i.e., the ice-dynamic contribution to sea level rise; Fig. 1c) show a much larger spread, with no clear correspondence to the climate forcing (Fig. 1b).

Sub-shelf melting in the ISMIP6 Antarctic 2300 model simulations is a function of the underlying melt parameterisation and the parameter values used. In designing a protocol for calculating sub-shelf melting for use in the ISMIP6 experiments, Jourdain et al. (2020) show that different calibration of the melt rate parameters to present-day melt rates can yield substantially different sensitivities in the melt rates to ocean thermal forcing changes, which translates to markedly different ice loss projections (Seroussi et al., 2020). The choice of an optimal set of parameters remains an open question. Approaches include matching to estimates of present-day melt rates based on remote sensing (Jourdain et al., 2020; Lazeroms et al., 2018; Reese et al., 2018a) or to ocean model simulations that capture interannual variability (Burgard et al., 2022; Jourdain et al., 2022), and fitting the sensitivity of melt rates to ocean temperatures estimated from oceanic surveys or ocean model projections (Reese et al., 2023). The use of parameterisations themselves might simplify or miss important processes, including the relevant ocean circulation (e.g., related to vertical structure in temperature, salinity and Coriolis). To circumvent this, ice sheet models can be forced by intermediate complexity melt rate models, such as the one-Layer Antarctic model for Dynamical Downscaling of Ice-ocean Exchanges (LADDIE; Lambert et al., 2023), or coupled with ocean models (e.g., the Marine Ice Sheet-Ocean Model Intercomparison Project; De Rydt et al., 2024). However, coupled ice sheet-ocean simulations are computationally expensive and currently unfeasible for large parameter space investigations or long timescales. Further questions related to the representation of ice shelf melt include the level of detail required for the sub-shelf melting representation to accurately simulate dynamic ice loss, as suggested by the variable importance of ice shelf regions for buttressing (Fürst et al., 2016; Reese et al., 2018b; Goldberg et al., 2019); and whether melt at the grounding line is most critical (e.g., Rignot and Jacobs, 2002; Seroussi et al., 2017) or if bulk melt rates are sufficient, as indicated in simulations of Pine Island Glacier (Joughin et al., 2021). In addition, ice sheet models might respond differently to ice shelf thinning, depending on, e.g., their representation of ice sheet basal sliding (e.g., Brondex et al., 2019; Cornford et al., 2020; Barnes and Gudmundsson, 2022), model resolution (e.g., Seroussi et al., 2017), and choices of sub-grid melting in the grounding zone (e.g., Seroussi and Morlighem, 2018).

Here, we aim to understand and disentangle how choices in the melt representation and ice sheet model influence the projected melt rates and resulting dynamic ice loss in the ISMIP6 Antarctic 2300 projections (Seroussi et al., 2024). Our specific objectives are to determine whether we can identify the source of uncertainty in: (i) the modelled basal melt rate, which is calculated from a common, prescribed ocean thermal forcing projections dataset; and (ii) the modelled ice loss in response to the applied basal mass balance forcing. To this end, we develop a melt sensitivity factor, which determines the melt rate response to a given change in ocean thermal forcing, and a dynamic ice loss sensitivity factor, which determines the dynamic ice loss and hence sea level contribution in response to the given cumulative sub-shelf melting anomaly. We assess the strengths and limitations of these sensitivity factors, applying them to explain uncertainties in projections of basal melt and dynamic ice loss in the ISMIP6 Antarctic 2300 ensemble.

https://doi.org/10.5194/egusphere-2025-4069
Preprint. Discussion started: 14 October 2025

2 Methods

2.1 ISMIP6 Antarctic 2300 experiments

We use outputs from the 16 modelling groups participating in ISMIP6 Antarctic 2300 (Seroussi et al., 2024). Amongst these, 12 different ice sheet models are represented. A total of 43 submissions were available for each climate forcing, representing a range of different stress balance approximations, mesh resolutions, initialisation procedures, and physical and numerical schemes, including melt rate parameterisations, sliding laws, and calving laws. A full description of the ice sheet models and the methods and data sets used to initialise them is provided in Seroussi et al. (2024).

Our analysis considers the degree to which the physical and numerical schemes – e.g., the melt rate parameterisation, initialisation procedure, resolution, and calving law – impact projections of melt rate and dynamic ice loss. Here, we briefly summarise the schemes that are relevant to our analysis (Table 1).

Table 1: Ice sheet model simulation features considered in our analysis. The melt rate parameterisations are: quadratic non-local (QNL); quadratic local (QL); quadratic non-local slope (QNLS); PICO; PICOP; and linear (Lin). The initialisation procedures are: DA; DA+; SP; and SP+. Calving parameterisations are: strain rate (SR); retreat only (RO); fixed front (FF); minimum thickness height (MH; as specified); von Mises (VM); and divergence and accumulated damage (Div). Melt is defined on partially-floating cells as: no melt (NO); melt (YES); a floating condition (FC); a sub-grid scheme (SG); or no partially-floating cells (N/A). The resolution of regridded model outputs varies from 4-32 km. The symbol * indicates the main submission per modelling group.

Model run	Melt param.	Initialisation	Calving	Partial melt	Resolution (km)
DC_ISSM	QNL	DA	MH (10 m)	SG	4
DOE_MALI_4km*	QNL	DA+	RO	FC	4
DOE_MALI_8km_Ant95	QNL	DA+	RO	FC	8
DOE_MALI_8km_AntMean	QNL	DA+	RO	FC	8
IGE_ElmerIce	PICO	DA+	FF	NO	4
ILTS_SICOPOLIS	QNL	SP+	MH (50 m)	FC	8
IMAU_UFEMISM1*	QL	SP+	FF	FC	32
IMAU_UFEMISM2	QL	SP+	FF	FC	32
IMAU_UFEMISM3	QL	SP+	FF	FC	16
IMAU_UFEMISM	QL	SP+	FF	FC	16
LSCE_GRISLI*	QNL	SP+	MH (200 m)	FC	16
LSCE_GRISLI2	QNL	SP+	MH (200 m)	NO	16
NCAR_CISM1	QNL	SP+	RO	SG	4
NCAR_CISM2*	QL	SP+	RO	SG	4

https://doi.org/10.5194/egusphere-2025-4069
Preprint. Discussion started: 14 October 2025

NORCE_CISM2	QNLS	SP+	RO	FC	4
NORCE_CISM3	QNLS	SP+	RO	FC	8
NORCE_CISM3_nonlocal*	QNL	SP+	RO	FC	8
NORCE_CISM3_local	QL	SP+	RO	FC	8
NORCE_CISM4	QNLS	SP+	RO	FC	16
NORCE_CISM4_nonlocal	QNL	SP+	RO	FC	16
NORCE_CISM4_local	QL	SP+	RO	FC	16
NORCE_CISM4_JRA	QNLS	SP+	RO	FC	16
NORCE_CISM5	QNLS	SP+	RO	FC	32
NORCE_CISM5_nonlocal	QNL	SP+	RO	FC	32
NORCE_CISM5_local	QL	SP+	RO	FC	32
PIK_PISM	PICO	SP	SR	FC	8
UCM_Yelmo	QNL	SP+	VM	SG	16
UCSD_ISSM	PICOP	DA	FF	SG	4
ULB_Kori1*	PICO	SP+	Div	NO	16
ULB_Kori2	QNL	SP+	Div	NO	16
UNN_Ua	QL	DA	RO	NO	4
UTAS_ElmerIce	QL	DA	FF	SG	4
VUB_AISMPALEO	QNL	SP	MH (50 m)	N/A	16
VUW_PISM1*	Lin	SP	SR	NO	8
VUW_PISM1_s1	Lin	SP	SR	NO	8
VUW_PISM1_s2	Lin	SP	SR	NO	8
VUW_PISM1_s3	Lin	SP	SR	NO	8
VUW_PISM1_s4	Lin	SP	SR	NO	8
VUW_PISM2	Lin	SP	SR	YES	8
VUW_PISM2_s1	Lin	SP	SR	YES	8
VUW_PISM2_s2	Lin	SP	SR	YES	8
VUW_PISM2_s3	Lin	SP	SR	YES	8
VUW_PISM2_s4	Lin	SP	SR	YES	8

A broad suite of melt rate parameterisations were used in ISMIP6 Antarctic 2300. First, a number of modelling groups used those developed for the ISMIP6 protocol (Jourdain et al., 2020; Favier et al., 2019). These melt parameterisations are based on local or non-local ocean properties, which are extrapolated into the ice shelf cavity from the surrounding ocean. These parameterisations have a quadratic relationship between ocean thermal forcing and melt, with parameters adjusted to match

https://doi.org/10.5194/egusphere-2025-4069
Preprint. Discussion started: 14 October 2025

observationally-derived melt rates. Variants are local, non-local (which includes an ice-shelf-averaged thermal forcing term to capture cavity-scale circulation), and non-local slope (which further includes a term for local ice shelf slope to improve melt rate predictions near grounding lines). Second, the Potsdam Ice-shelf Cavity mOdel (PICO; Reese et al., 2018a), which simulates the impact of the overturning circulation on individual ice shelves, or a modified version of PICO that incorporates plume dynamics (PICOP; Pelle et al., 2019) were used by four groups. Finally, one group used a melt rate parameterisation that linearly depends on the prescribed thermal forcing (Martin et al., 2011). For more detail on the different melt parameterisations and their performance in matching melt rates simulated by ocean models, we refer to Burgard et al. (2022).

The initialisation procedures were broadly categorised as data assimilation or spin-up. Data assimilation (DA) procedures involved tuning of unknown variables (e.g., the basal friction coefficient or the ice rigidity) via snapshot inversion (as opposed to transient calibration) to reduce the misfit between simulated and observed fields, typically the ice surface velocity. A number of model simulations used data assimilation followed by a relaxation period (denoted DA+). Spin-up (SP) initialisation comprised methods that evolved the geometry and dynamics over a long period until a steady-state was reached, potentially following up with simulations using paleo-climate or historic forcing, and sometimes including optimisation of unknown fields (e.g., basal friction and ice rigidity). A number of models used spin-up procedures that included ice thickness target values (SP+; Pollard and DeConto, 2012). Melt was applied differently in the grounding zone depending on whether there were partially-floating grid cells, as follows: no melt applied on partially-floating cells (NO); melt applied on partially-floating cells (YES); melt applied using a floating condition (FC); melt applied using a sub-grid scheme (SG; e.g., Seroussi and Morlighem, 2018); or no partially-floating cells (N/A).

Some models simulate iceberg calving based on: strain rate (SR; Levermann et al., 2012), minimum thickness height (MH; values for the minimum thickness height as specified from Seroussi et al., 2024), von Mises (VM), and divergence and accumulated damage (DV; Pollard et al., 2015). Other models have a fixed front (FF), or allow retreat only if local mass balance thins ice thickness to zero (RO). All ice sheet model outputs were interpolated onto a regular grid at a resolution close to the models' native resolutions, namely 4, 8, 16, or 32 km.

We restrict our analysis to four high-emission scenario experiments: exp02-exp05. These experiments are forced with climate outputs (ocean and atmosphere) from the CCSM4, HadGEM2-ES, CESM2-WACCM, and UKESM1-0-LL General Circulation Model simulations over the period 2015-2300 (Nowicki et al., 2020; Barthel et al., 2020). The CCSM4 and HadGEM2-ES models use the Representative Concentration Pathway 8.5 (RCP8.5) scenario from the Coupled Model Intercomparison Project 5 (CMIP5, Taylor et al., 2012); CESM2-WACCM and UKESM1-0-LL use the Shared Socioeconomic Pathway 5-8.5 (SSP5-8.5) scenario from CMIP6 (Eyring et al., 2016). We also consider the control experiment – in which the climate forcings remain constant from 2015-2300 and are similar to the climate conditions over the period 1995-2014 – to calculate the anomaly of the dynamic sea level contribution (dSLR; see section 2.3.1). We do not include the ISMIP6 experiments of ice shelf collapse in our analysis.

Ice sheet model simulation outputs comprise 2-dimensional fields, including ice sheet geometry, flow, and applied forcings. We consider differences over the whole Antarctic Ice Sheet and in sector-wide behaviours by analysing outputs over the Amundsen Sea sector, Filchner-Ronne sector, Aurora Subglacial Basin, Wilkes Subglacial Basin, and Ross Sea sector. Here,

https://doi.org/10.5194/egusphere-2025-4069
Preprint. Discussion started: 14 October 2025

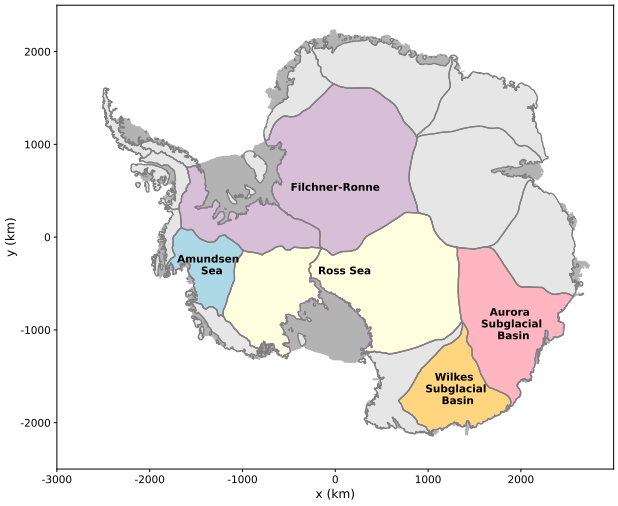

Figure 2. Sectors used in the analysis, identified following IMBIE2 conventions (Shepherd et al., 2018), as follows: Amundsen Sea sector (G-H), Filchner-Ronne sector (J-Jpp and Jpp-K), Aurora Subglacial Basin (Cp-D), Wilkes Subglacial Basin (D-Dp), and Ross Sea sector (Ep-F and E-Ep).

we define the Filchner-Ronne sector as the combination of basins J-Jpp and Jpp-K from the Ice sheet Mass Balance Intercomparison Exercise 2 (IMBIE2 Shepherd et al., 2018), and the Ross sector as the combination of basins Ep-F and E-Ep from IMBIE2. The sectors of interest used in our analysis are highlighted in Fig. 2.

Prior to calculating the variables used in our analysis, we perform data exploration and visualisation of the ice sheet model output. A full description of this quality control is provided in appendix A. During our analysis, we identified inconsistencies and missing data in the output of several ice sheet models. We list these and the corrections made in appendix B.

2.2 Determining the thermal forcing

Each ice sheet model simulation was forced using an ocean thermal forcing dataset derived from the four experiments (exp02-exp05). The ocean forcing datasets were provided to the ice sheet modelling groups as 4-dimensional thermal forcing fields in space (x, y, z) and time (t), extrapolated to any location over the Antarctic continent that is currently not occupied by the ocean, i.e., over grounded ice or in the bedrock (Jourdain et al., 2020). As each ice sheet model's geometry was initialised differently and evolved differently over time (via changes in shelf draft and grounding line position), the thermal forcing acting directly on the ice shelf base varied across models and experiments; however, the specific ice sheet model thermal forcing field was not provided as standard output in the ISMIP6 output suite. To determine the thermal forcing acting on the ice shelf base in each simulation, we linearly interpolated the thermal forcing from the climate dataset onto the ice sheet model grid, deriving

https://doi.org/10.5194/egusphere-2025-4069
Preprint. Discussion started: 14 October 2025

a thermal forcing value at the ice shelf draft for each ice sheet model grid cell. This resulted in a 3-dimensional dataset (x, y, t) of thermal forcing beneath each ice shelf for each time step over the entire simulation period 2015-2300.

We acknowledge that this thermal forcing field may differ slightly from the field used to force the model due to differences in: the grid resolution of the output models compared with their native grid resolution; the interpolation of thermal forcing onto the ice shelf draft; and the melt rate parameterisations used – e.g., the ice sheet models that use PICO for the melt rate parameterisation rely on far-field near-sea-floor temperatures rather than extrapolated 3-dimensional thermal forcing fields. However, our approach uses a single method to estimate the thermal forcing across all models, allowing for a more consistent comparison, and we anticipate that the calculated thermal forcing field should be a reasonable approximation for the purposes of our analysis. The calculated 3-dimensional thermal forcing field was then used to calculate the time series of average thermal forcing over the different sectors, as detailed in the following subsection.

2.3 Time series analysis

To investigate the different sectors of interest (Fig. 2), we compare time series of the basal melt rate, basal mass balance, thermal forcing, ice shelf geometry, and dynamic sea level anomaly. The time series are obtained by averaging or integrating within these specific sectors (Section 2.3.1). We also calculate the basal melt rate time series across different depth levels to investigate melt rate depth profiles (Section C1), and in regions near the grounding line (Section C2).

2.3.1 Time series

We analyse the following one-dimensional time series provided by Seroussi et al. (2024) for each ice sheet model and experiment: total basal mass balance (BMB), floating ice shelf area, and grounded ice sheet area. For the Ross and Filchner-Ronne sectors, variables from the two basins comprising each sector were added to create a combined time series (Fig. 2). Average basal melt was calculated by dividing the BMB by the shelf area for each sector.

To determine the average thermal forcing within each sector, we created 1-dimensional time series analogous to Seroussi et al. (2024) for each sector. We averaged the 3-dimensional (x, y, t) thermal forcing fields within the ice mask and floating area of the ice sheet model for each sector.

We generated dynamic sea level anomaly time series to isolate the dynamic ice loss contributions (i.e., contributions arising from ice-dynamic discharge) from the total sea level contributions for the Antarctic and each sector. These are calculated by subtracting the grounded SMB anomaly (experiment minus control) from the volume above flotation anomaly (experiment minus control). We note that this allows us to determine the contribution of dynamic ice loss to the full sea level response, which is different from running experiments directly without surface mass balance changes to understand the dynamic response in the absence of surface mass balance forcing.

https://doi.org/10.5194/egusphere-2025-4069
Preprint. Discussion started: 14 October 2025

2.4 Melt and dynamic ice loss sensitivity factors

2.4.1 Linear melt sensitivity factor

Each ice sheet model simulation uses a distinct melt parameterisation and individual parameters in that parameterisation, resulting in significant variations in basal melt evolution over time (Fig. 1b). To facilitate comparison of basal melt evolution among the model simulations, we derive a melt sensitivity (MS) factor for each model simulation. This factor indicates how much the basal melting changes for a given change in thermal forcing.

The MS factor is approximated as the slope obtained by a linear regression between shelf-average basal melt relative to the control simulation, $\frac{\Delta\text{BMB}}{\Delta\text{Shelfarea}}$, versus average thermal forcing relative to the control simulation, ΔTF (K), calculated for each model simulation:

$$\frac{\Delta\text{BMB}(t)}{\Delta\text{Shelfarea}(t)} = \text{MS}\,\Delta\text{TF}(t) + c, \tag{1}$$

where c is the intercept of the linear regression.

Thus, we can predict the total change in basal mass balance of a sector, ΔBMB_predict, given the thermal forcing anomaly relative to the control run and the ice shelf area evolution over time as:

$$\Delta\text{BMB\_predict}(t) = \text{MS}\,\Delta\text{TF}(t)\,\Delta\text{Shelfarea}(t) + c\,\Delta\text{Shelfarea}(t). \tag{2}$$

The goodness-of-fit of the MS factor was assessed by calculating the percentage root mean square error between the actual and predicted ΔBMB (supporting Fig. S1). BMB generally increases at the start of the experiment, but may experience a sudden decrease due to loss of ice shelf area triggered by model-specific calving events (Fig. 1b). For instance, the total BMB across Antarctica for the UKESM-forced scenarios decreases around 2150 for most models. These abrupt changes make it challenging to maintain a consistent MS. To address this, we limited the MS fitting to data prior to the point of maximum basal mass balance $t = t(\text{BMB\_max})$, where calving effects are minimal.

While our method performed well for most ice sheet models (e.g., see Antarctic results for exp02 in supporting Fig. S2), in some cases the predicted basal mass balance evolution deviated significantly from the actual trend. A closer inspection suggested that fitting earlier in the simulation period might yield a better match. Consequently, in addition to our original fitting method (i) up to $t = t(\text{BMB\_max})$, we assessed two other fitting strategies: (ii) up to $t = \min(t(\text{BMB\_max}), t(\text{TF} \leq 2K))$, and (iii) up to $t = \min(t(\text{BMB\_max}), 2100)$. An example of these three methods applied to the NORCE_CISM5_local model simulation in the Aurora sector is shown in supporting Fig. S3. Note that we also tested fitting a quadratic dependence of TF in Eq. 1, which resulted in a much poorer fit.

For each ice sheet model simulation, experiment, and sector of interest, we determined the MS using all three methods (i-iii) and calculated the percentage root mean square error for all four climate experiments. We then averaged the percentage root mean square error across all sectors to obtain a mean percentage root mean square error for each method. The method with the lowest mean percentage root mean square error was selected as the MS factor determination method for each model simulation (supporting Fig. S4). Although the chosen method may vary across model simulations, it remains con-

https://doi.org/10.5194/egusphere-2025-4069
Preprint. Discussion started: 14 October 2025

sistent across sectors within a given model simulation. Most MS factors are derived using the first method (i); the models NORCE_CISM5_local, NORCE_CISM5, IMAU_UFEMISM3 and IMAU_UFEMISM4 are derived using method (ii); and IMAU_UFEMISM1 IMAU_UFEMISM2 with method (iii). We generated uncertainty estimates from the range between the minimum and maximum MS values determined across the four different climate forcing experiments. The mean MS factors across the experiments are those referred to throughout the rest of the analysis.

For the quadratic local and non-local melt rate parameterisations – where the melt rate is a quadratic function of thermal forcing – higher thermal forcing values will result in higher MS factors for a given constant heat exchange coefficient (γ). This is not necessarily the case for the quadratic parameterisations that include slopes or a variable γ, neither is it the case that a non-quadratic formula will necessarily have a lower MS factor than a quadratic formula.

2.4.2 Linear dynamic ice loss sensitivity factor

To assess the relationship between the basal mass balance projections and the simulated dynamic ice mass loss (Fig. 1), we derived a dynamic ice loss sensitivity (DS) factor. In a similar vein to the MS factor, this factor indicates how much the dynamic ice loss changes for a given change in ice shelf basal mass balance.

The DS factor approximates the dynamic ice mass loss (Gt) relative to the control simulation using the cumulative basal mass balance (Gt) relative to the control simulation for each ice sheet model simulation. We calculated the DS factor for the Antarctic and each sector by performing a linear regression to obtain a slope and intercept of cumulative basal mass balance anomaly versus dynamic ice mass loss, where the slope represents the DS factor similar to Eq. 1. Thus, the dynamic ice mass loss anomaly can be predicted from the basal mass balance anomaly using the following equation:

$$\Delta\,\mathrm{DIML\_predict}(t) = \mathrm{DS} \int_0^t \Delta\,\mathrm{BMB}(t')\,dt' + d, \tag{3}$$

where DIML is the dynamic ice mass loss anomaly (Gt) and d is the intercept of the linear regression. The uncertainty in the DS factors for the Antarctic and by sector was calculated as the spread in the estimated slope of the linear regression in Eq. 3 for each of exp02-exp05.

The goodness of fit of the DS for Eq. 3 was assessed by calculating the percentage root mean square error between the actual and predicted dynamic ice mass loss (see Fig. S5). Regressing the variables from 2150-2300 resulted in the lowest percentage root mean square error, while still ensuring a long enough time series to establish statistical significance. Including years prior to 2150 resulted in an overestimation of the sensitivity for most models due to a change in slope in the dynamic ice mass loss over the first 150 years of simulation. A linear fit over 2150-2300 generally resulted in a percentage root mean square error value of <25% for the aggregated Antarctic data (Fig. S5). The four IMAU members had percentage root mean square error values >65% due to strongly variable dynamic ice mass loss in the final ∼80 years of simulation, which reduced the reliability of the linear fit. The percentage root mean square error values were also generally higher in the Aurora and Wilkes sectors for models that simulated a marked change in slope in the dynamic ice mass loss in the final ∼80 years of simulation to 2300.

https://doi.org/10.5194/egusphere-2025-4069
Preprint. Discussion started: 14 October 2025

2.5 Analysis of variance (ANOVA)

To analyse the influence of different sources of uncertainty on basal mass balance evolution and dynamic sea level contribution, we performed an analysis of variance (ANOVA; Girden, 1992; von Storch and Zwiers, 2002) similar to Seroussi et al. (2023, 2024). We tested the role of factors such as the climate forcing, the melting, calving, and modelling choices on the variance of basal mass balance and dynamic sea level rise, respectively. We used the MATLAB function `anovan` with the interaction model and square sum type 1 to determine the ANOVA, assuming fixed effects (since we are only interested in statements about the finite, represented number of factor levels, e.g., the four different climate forcing experiments analysed here). Using ANOVA, we split the full variance into the variance of individual factors and their interactions to understand which factor contributed most to the uncertainty in melt or dynamic ice loss. We only tested the main submission of each ice sheet modelling group to avoid double counting – a total of 64 simulations.

We also use the Kruskal-Wallis H-test (or one-way ANOVA on ranks; Kruskal and Wallis, 1952) to investigate the extent to which the MS and DS factors depend on underlying model assumptions. Specifically, we consider the categories of model resolution, melt rate parameterisation, calving procedure, and initialisation procedure, and test whether the median MS and DS factors for each grouping are statistically significantly different. We do not separately consider melt on partially floating cells due to the small number of models in some of the categories that prevents statistical significance from being established.

3 Results

We first analyse the projected basal mass balance in the ensemble (Section 3.1), then its influence on the projected dynamic sea level contributions (Section 3.2).

3.1 Basal mass balance projections

We start by analysing the links between thermal forcing and modelled basal mass balance (Fig. 1a, b). The evolution of the total basal mass balance is expected to be roughly governed by the evolution of the ice shelf area and the melt sensitivity. We hence first investigate the melt sensitivity factor (section 3.1.1), and then the influence of the calving representation on the evolution of shelf area (section 3.1.2) and basal mass balance (section 3.1.3), as well as the other sources of uncertainty in the modelled basal mass balance (section 3.1.4).

3.1.1 Melt sensitivity factors

The MS factors are an indicator of the magnitude of the melt rate change for a given thermal forcing change; hence we expect that simulations with higher MS factors generally project higher melt rates. We first examine how the MS factors vary by ice sheet model simulation and sector (Fig. 3; table 2).

https://doi.org/10.5194/egusphere-2025-4069
Preprint. Discussion started: 14 October 2025

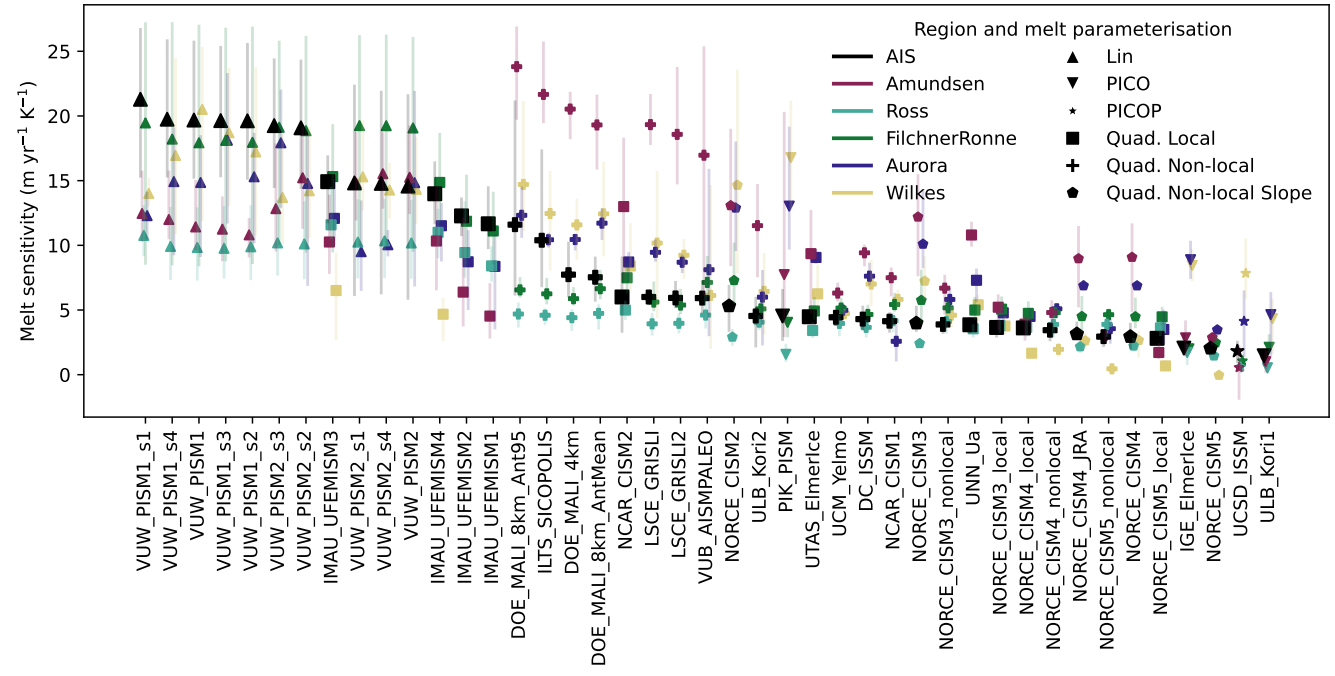

Figure 3. Melt sensitivity (MS) factor ($\mathrm{m\,yr^{-1}\,K^{-1}}$) for different ice sheet model simulations and sectors. The markers represent the experiment-averaged MS factor for each ice sheet model simulation and sector. The sectors are: the Antarctic (black), Amundsen Sector (purple), Ross Sector (cyan), Filchner-Ronne Sector (green), Aurora Subglacial Basin (dark blue), and Wilkes Subglacial Basin (yellow). Thin coloured lines indicate the maximum and minimum MS factors derived from experiments exp02-exp05. Ice sheet model simulations on the x-axis are ordered by their Antarctic MS factor in descending order. Different markers denote the melt parameterisation used by each model: linear (upward triangle), PICO (downward triangle), PICOP (star), quadratic local (square), quadratic non-local (plus), and quadratic non-local slope (pentagon).

Table 2: Summary of key results for each ice sheet model simulation, including the: average, minimum and maximum Antarctic-wide MS factors ($\mathrm{m\,yr^{-1}\,K^{-1}}$); calving group; and average, minimum, and maximum Antarctic-wide DS factors. The MS factors are defined according to Eq. 1; the minimum and maximum values are calculated by comparing the MS factors across the experiments (climate forcing scenarios). The calving group is defined in Section 3.1.2 and comprises: strong calving (1); moderate calving or otherwise (2). The DS factors are defined according to Eq. 3, and minimum and maximum values calculated from the experiments (climate forcing scenarios).

Model	MS	MS min	MS max	Calving group	DS	DS min	DS max
DC_ISSM	4.3	3.5	5.2	2	0.1	0.1	0.2
DOE_MALI_4km	7.7	6.1	10.2	2	0.5	0.4	0.7
DOE_MALI_8km_Ant95	11.6	6.2	21.1	2	0.5	0.5	0.6

https://doi.org/10.5194/egusphere-2025-4069
Preprint. Discussion started: 14 October 2025

DOE_MALI_8km_AntMean	7.5	5.8	9.0	2	0.5	0.4	0.6
IGE_ElmerIce	2.1	1.6	3.1	2	0.1	0.0	0.1
ILTS_SICOPOLIS	10.4	6.9	17.3	2	0.6	0.5	0.7
IMAU_UFEMISM1	11.7	9.8	14.5	2	2.4	0.8	4.0
IMAU_UFEMISM2	12.3	10.8	13.6	2	2.6	1.1	4.6
IMAU_UFEMISM3	14.9	11.8	16.8	2	2.1	1.3	3.5
IMAU_UFEMISM4	14.0	11.7	16.4	2	2.2	1.3	3.7
LSCE_GRISLI	6.0	5.5	6.3	1	1.1	0.7	1.6
LSCE_GRISLI2	5.9	5.3	7.1	1	0.3	0.3	0.3
NCAR_CISM1	4.1	3.4	4.7	2	0.2	0.2	0.2
NCAR_CISM2	6.0	3.3	9.0	2	0.6	0.4	0.7
NORCE_CISM2	5.3	3.4	6.8	2	0.5	0.4	0.7
NORCE_CISM3	4.0	3.4	5.2	2	0.6	0.4	0.7
NORCE_CISM3_local	3.7	3.0	4.1	2	0.3	0.2	0.4
NORCE_CISM3_nonlocal	3.9	3.3	4.3	2	0.3	0.2	0.5
NORCE_CISM4	2.9	2.1	3.9	2	0.6	0.4	0.8
NORCE_CISM4_local	3.6	3.2	4.0	2	0.4	0.3	0.6
NORCE_CISM4_nonlocal	3.4	2.7	3.9	2	0.4	0.2	0.6
NORCE_CISM4_JRA	3.1	2.8	4.0	2	0.6	0.4	0.8
NORCE_CISM5	2.0	1.7	2.6	2	0.5	0.3	0.8
NORCE_CISM5_local	2.8	2.3	3.2	2	0.5	0.3	0.7
NORCE_CISM5_nonlocal	2.9	2.2	3.4	2	0.5	0.3	0.8
PIK_PISM	4.5	2.7	6.5	1	0.9	0.8	0.9
UCM_Yelmo	4.4	4.3	4.8	1	0.5	0.4	0.7
UCSD_ISSM	1.8	1.0	2.5	2	0.1	0.1	0.3
ULB_Kori1	1.5	0.8	1.8	2	0.4	0.2	0.5
ULB_Kori2	4.5	2.2	5.9	2	0.5	0.5	0.5
UNN_Ua	3.9	3.3	4.3	2	0.4	0.3	0.5
UTAS_ElmerIce	4.5	4.1	4.9	2	0.1	0.1	0.2
VUB_AISMPALEO	5.9	4.9	7.2	2	0.3	0.0	1.2
VUW_PISM1	19.7	15.3	25.7	1	0.5	0.5	0.6
VUW_PISM1_s1	21.3	15.3	26.7	1	0.4	0.0	0.6
VUW_PISM1_s2	19.6	15.2	25.5	1	0.5	0.5	0.5
VUW_PISM1_s3	19.6	15.4	25.3	1	0.5	0.4	0.5
VUW_PISM1_s4	19.8	15.3	25.8	1	0.6	0.5	0.7

https://doi.org/10.5194/egusphere-2025-4069
Preprint. Discussion started: 14 October 2025

VUW_PISM2	14.6	5.9	21.6	1	0.7	0.6	0.8
VUW_PISM2_s1	14.8	6.2	22.3	1	0.7	0.6	0.9
VUW_PISM2_s2	19.1	14.5	24.2	1	0.6	0.6	0.7
VUW_PISM2_s3	19.3	14.5	24.3	1	0.6	0.5	0.7
VUW_PISM2_s4	14.8	6.3	21.8	1	0.7	0.6	0.8

The spread of MS factors for the entirety of the Antarctic ice shelves varies by a factor of around 15 between the different ice sheet model simulations (from 1.5 $\mathrm{m\,yr^{-1}\,K^{-1}}$ for ULB_Kori1 to 21.3 $\mathrm{m\,yr^{-1}\,K^{-1}}$ for VUW_PISM_s1). Considering the individual sectors, the largest MS factors occur for the Amundsen sector with values ranging from 0.55 $\mathrm{m\,yr^{-1}\,K^{-1}}$ to 21.85 $\mathrm{m\,yr^{-1}\,K^{-1}}$. For 19 out of the total 43 model configurations, the Amundsen Sea has the highest MS values amongst sectors. In other cases, the Antarctic-wide average (8/43), or the Filchner-Ronne (8/43), Wilkes (4/43), or Aurora (4/43) sectors have the highest values. For most models, the lowest MS factors are often evidenced in the Ross sector (28/43), sometimes in Wilkes sector (7/43), and to a lesser extent in the Aurora sector (3/43), Amundsen sector (3/43), or for the whole ice sheet (2/43). MS factors for Filchner-Ronne sector range from 1.1 $\mathrm{m\,yr^{-1}\,K^{-1}}$ to 19.5 $\mathrm{m\,yr^{-1}\,K^{-1}}$, values for the Ross sector from 0.5 $\mathrm{m\,yr^{-1}\,K^{-1}}$ to 11.6 $\mathrm{m\,yr^{-1}\,K^{-1}}$, for the Aurora sector from 2.6 $\mathrm{m\,yr^{-1}\,K^{-1}}$ to 18.1 $\mathrm{m\,yr^{-1}\,K^{-1}}$ and for the Wilkes sector from 0.0 $\mathrm{m\,yr^{-1}\,K^{-1}}$ to 20.5 $\mathrm{m\,yr^{-1}\,K^{-1}}$.

There is no consistent pattern in the MS factor magnitude and associated uncertainty (i.e., variability of MS values across the experiments, shown as lines in the figure), although the models with higher Antarctic MS factors tend to have larger differences between the experiments, see also Fig. S6. Averaging the Antarctic-wide MS factor for each climate forcing scenario (exp02-exp05) overall all model simulations does not reveal a clear pattern: there is no climate model forcing that consistently yields a higher MS factor for all ice sheet model simulations (supporting Fig. S6). Since the averages per experiment (supporting Fig. S6, dashed line) for exp02-exp05 are similar, this supports our method of choosing one average MS factor across all experiments as a fair comparison between the ice sheet model simulations.

We consider the extent to which the MS factors for each sector can be predicted based on: the melt parameterisation, calving mechanism, initialisation procedure, or model resolution (see Fig. S7). Although we do find differences in the melt sensitivity with respect to these different classifiers, in general we cannot clearly link the magnitude of the MS factor to any single model choice, and the small sample size prevents us from establishing robust statistical significance. For example, while there appears to be a statistically-significant difference in the MS factor for the linear melt parameterisation in comparison to other parameterisations, only one of the ice sheet models (VUW_PISM; eight ensemble members) uses the linear melt parameterisation, and it not clear that the MS factor value for this model is due to the melt parameterisation or other factors. We further discuss the issue of uncertainty with respect to model parameters in Section 4.

https://doi.org/10.5194/egusphere-2025-4069
Preprint. Discussion started: 14 October 2025

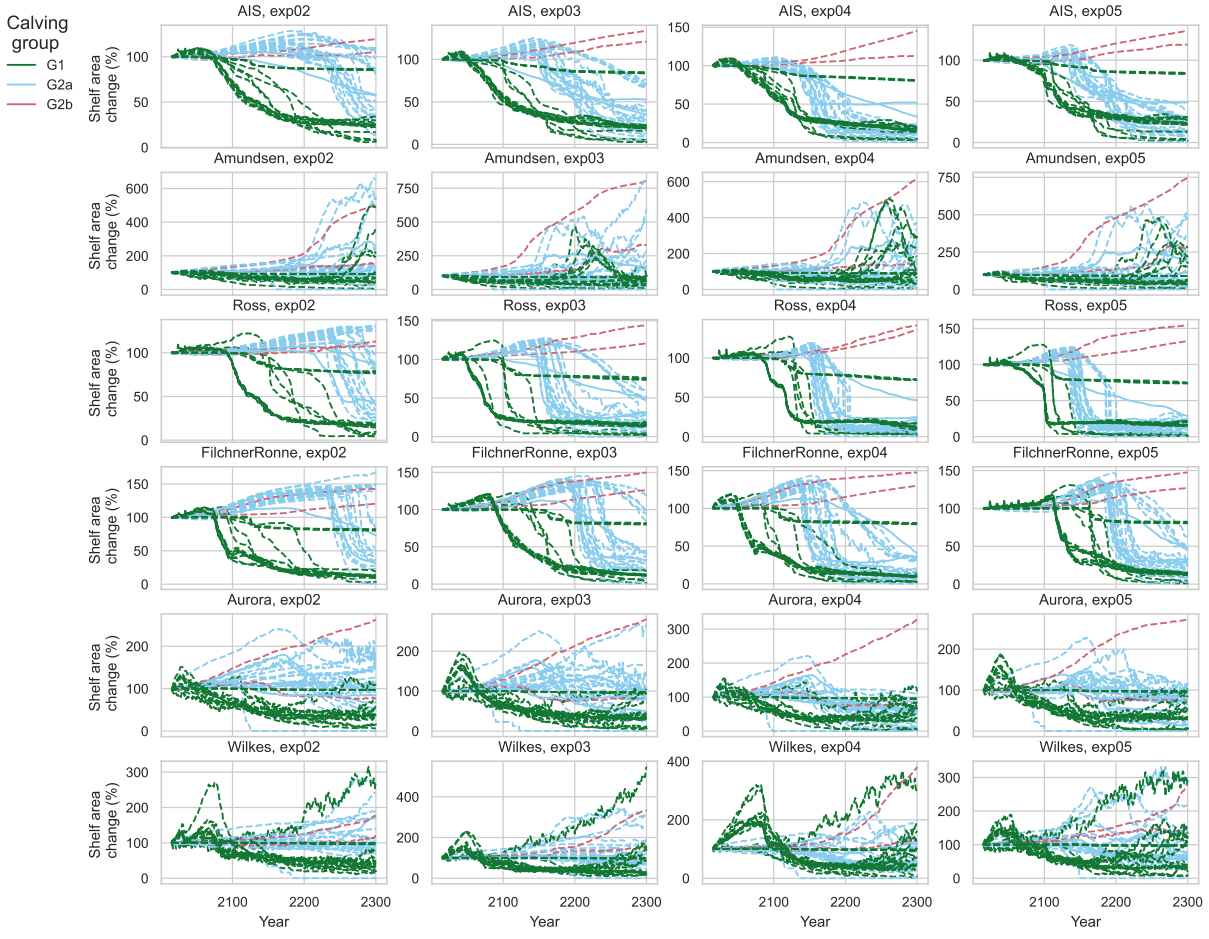

Figure 4. Relative shelf area changes (%) from 1995 to 2300 for different sectors of the Antarctic Ice Sheet, including the Amundsen Sea sector, Ross Ice Shelf, Filchner-Ronne Ice Shelf, Aurora Subglacial Basin, and Wilkes Subglacial Basin (from top to bottom). Columns represent results from different experiments (exp02-exp05) from left to right. The relative shelf area change is expressed as a percentage of the initial shelf area. The colours represent two model groupings: group 1 (G1; green) consists of models with strong calving; group 2 (G2a; light blue) includes models with moderate calving. The two brown lines (G2b) represent the two models from group 2 with a fixed calving front and no post-processing to remove shelf area.

https://doi.org/10.5194/egusphere-2025-4069
Preprint. Discussion started: 14 October 2025

3.1.2 Influence of ice shelf area changes

Given that the basal mass balance is influenced by the ice shelf area, we next consider the evolution of the ice shelf area from 1995-2300 (Fig. 4). Aggregated for all Antarctic ice shelves, the ice shelf area changes in the first 25 years of simulation are generally small. During this period, most models simulate a slight increase in the shelf area, consistent with grounding line retreat that is also indicated by a consistent decline in the grounded area (Figs. S9 and S10). However, after this initial period, shelf area changes vary markedly between ice sheet model simulations, and two distinct categories of behaviours emerge: model simulations that simulate strong calving show ice shelf area changes within 100 years of the simulation (SR, VM or MH=200 m calving procedures); model simulations that simulate moderate calving (RO, MH$\leq$50 m, Div), or have no movement of the calving front (FF), show initial ice shelf growths indicating grounding line retreat with later (after year 2150) or no decline in ice shelf area. The same behaviour is seen for all four experiments, although there are differences in timing of ice shelf area decline. Hence, we introduce a calving group category that allows us to categorise these two shelf area behaviours over time (see Table 2). Note that our categories are qualitative, and not a statistically robust means of differentiating the model responses or linking them to specific modelling choices to establish causality. We define the groups based on the ice shelf area changes, where we attribute large-scale and sudden decreases in ice shelf area to calving (potentially supported by strong melting). However, this often co-occurs with increasing shelf area due to grounding line retreat (compare Fig. 4 with Figs. S9 and S10), such that a constant shelf area can either hint at no ongoing changes or a balance of area gained by retreat and lost by calving and melting.

The behaviours of group 2 models are most clearly distinguished from group 1 model simulations in the Ross and Filchner-Ronne sectors, and to a lesser extent in the Aurora sector. There is a relatively broad spread of behaviours in shelf area change between models in group 2. Two models in group 2 – ULB_Kori1 and UCSD_ISSM – consistently predict shelf area increases throughout the simulation period for almost all sectors. The increases are most notable in the Amundsen, Ross, Filchner-Ronne and Aurora sectors, and tend to be larger in exp03-exp05 than in exp02. Note that other models with fixed ice front (see Table 1; IGE_Elmer/ice, IMAU_UFEMISM, Utas_Elmer/ice), have post-processed their ice shelf mask to remove areas with a certain minimum thickness, therefore showing declining ice shelf area. These two models (ULB_Kori1 and UCSD_ISSM) did not undergo this post-processing and we anticipate that they would have a similar behaviour to other group 2 models if post-processing was carried out.

In general, our grouping category does not yield distinguishable differences in the Amundsen and Wilkes sectors. Here, calving does not seem to play a major role in determining the shelf area. In particular, in the Amundsen sector, a number of models simulate consistent increases in ice shelf area beyond 2100 – with increases as high as 600% by the end of 2300 in some cases – and the remainder of the ice sheet models show relatively little to no change indicating a balance between shelf area growth through grounding line retreat, and shelf area loss through calving and melting. Marked shelf area growth in the Amundsen sector is consistent with strong grounding line retreat as shown by a decline in the grounded area (Fig. S9). There is little evidence of significant calving in the Amundsen sector as there is no rapid and high magnitude decrease in shelf area across the entire simulation period. Shelf area changes in the Wilkes sector vary considerably between models, with both ice

https://doi.org/10.5194/egusphere-2025-4069
Preprint. Discussion started: 14 October 2025

shelf growth or reduction. There is a relatively smaller spread of shelf area difference between models in the Wilkes and Aurora sectors than in other sectors, although several models show large shelf area increases here.

We assess the links between MS and shelf area evolution and find no general trend between MS and the shelf area behaviour across models. However, where multiple simulations were submitted from the same modelling group, simulations that have higher MS factors also consistently show a larger, and more rapid, increase in ice shelf area than the simulations with lower MS factors consistent with higher melting driving faster grounding line retreat. This is the case, for example, with the NORCE-CISM model (Fig. S11), where the simulations with the highest MS consistently yield the highest shelf area growth.

In summary, calving strongly affects the shelf area evolution in most sectors and some broad categorisations can be made. However, the calving group is a less robust predictor of ice shelf changes for the Amundsen and Wilkes sectors.

3.1.3 Evolution of basal mass balance

Broadly, the basal mass balance evolution is governed by the MS factor and the evolution of the ice shelf area changes, see Sect. 2.4.1. In the previous section, we discussed that there is no general relationship between MS and calving group. We now analyse how calving group and MS influence the BMB evolution in the ensemble.

The change in total basal mass balance over time is plotted using the same grouping by calving category as Section 3.1.2, see Fig. 5. We find similar results to the shelf area changes: While the calving group distinguished well between mass balance evolution for the entire Antarctic, the Ross and FRIS sectors, it proves less effective at distinguishing between model behaviours in the Amundsen, Aurora and Wilkes sectors where smaller ice shelves are present today. In the Aurora sector, some model simulations (predominantly the VU_PISM ensemble) in group 1 exhibit a growth in BMB in the first $\sim$100 years of simulation (Fig. 5, black lines), in contrast to the remaining group 1 models, where strong calving behaviour reduces the shelf area (and hence total BMB). In the Amundsen and Wilkes sectors, calving plays a less significant role as already discussed in Section 3.1.2.

In the sectors where the calving group is less useful to predict the basal mass balance evolution, we investigate correlations between the MS factor and total melt change by 2300 (Fig. 6). For the Wilkes sector, we find a statistically significant relationship between the MS factor and the total melt change across all experiments; for most experiments, BMB remains relatively stable over time, with little overall decline (Fig. S12). In contrast, the Amundsen sector displays a unique behaviour in experiment exp03, with an early BMB peak followed by a decline – likely due to early calving onset (Fig. S12). This is also the only experiment in which we do not observe a statistically significant linear relationship between the MS factor and total melt change. These results suggest that the MS factor is a reliable predictor of total melt over the simulation period to 2300 for these two sectors (for the other sectors we found no statistically significant influence of MS on total BMB as we think this is obscured by the calving behaviour).

To summarise, we find that for the Filchner-Ronne and Ross sectors, basal mass balance evolution is dominated mainly by the calving group, while for the sectors with small ice shelves at present, basal mass balance evolution is explained solely by the MS factor.

https://doi.org/10.5194/egusphere-2025-4069
Preprint. Discussion started: 14 October 2025

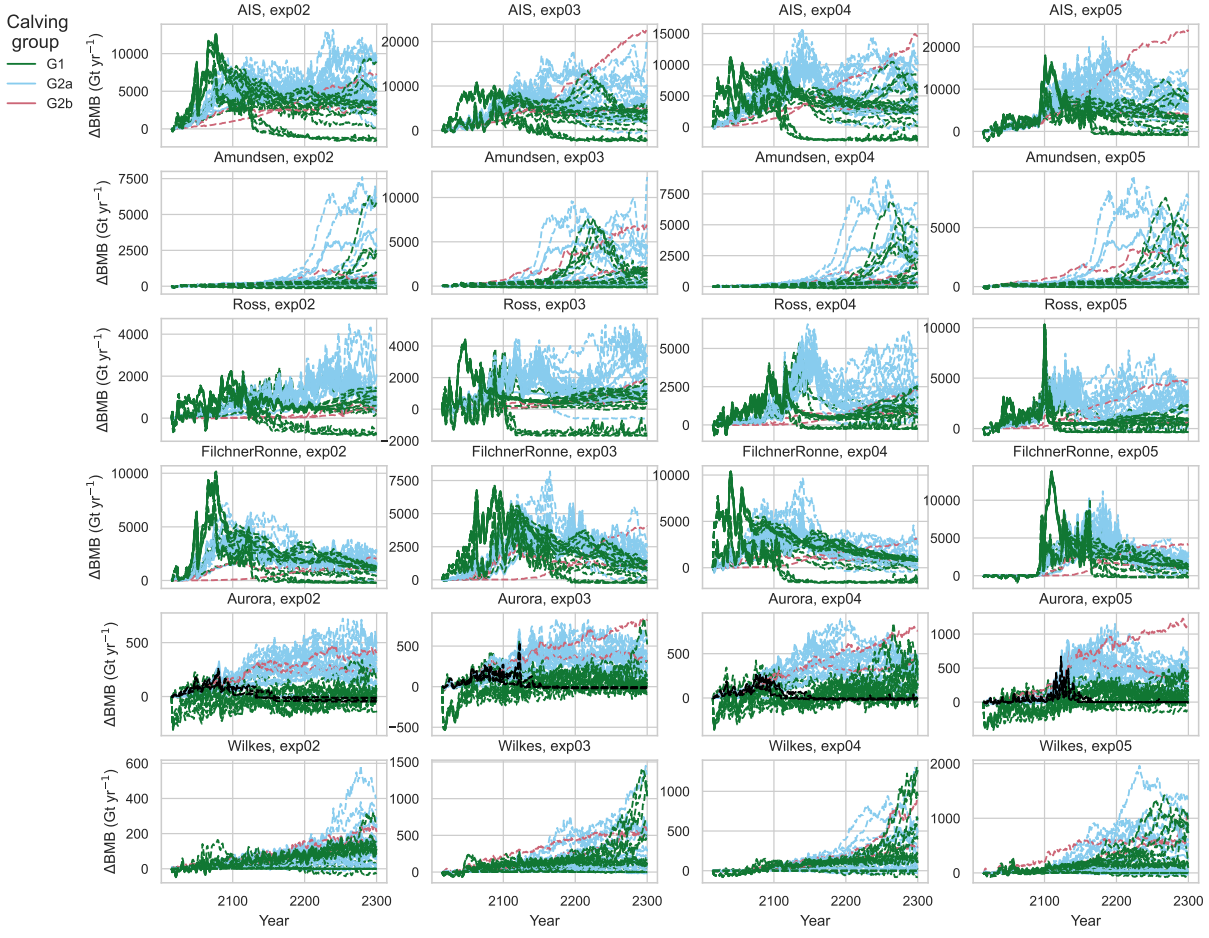

Figure 5. Same as Fig. 4, but showing changes in the total ΔBMB (i.e. BMB calculated with respect to the control) over time ($\mathrm{Gt\,yr^{-1}}$). Colours are the same as in Fig. 4, but the black lines in the Aurora sector represent simulations from the VUW-PISM ensemble.

3.1.4 Uncertainties in basal mass balance

We analyse the factors that contribute to uncertainty in the projected basal mass balance. We use the categorical factors "climate", "melt sensitivity" and "calving", defined as follows. The "climate" factor categorises model runs with the four different climate forcings (experiments exp02-exp05). To establish the factor levels for the "melt sensitivity" we create five bins, with: (i) very low sensitivity being smaller than the mean sensitivity minus one standard deviation; (ii) low sensitivity being higher

https://doi.org/10.5194/egusphere-2025-4069
Preprint. Discussion started: 14 October 2025

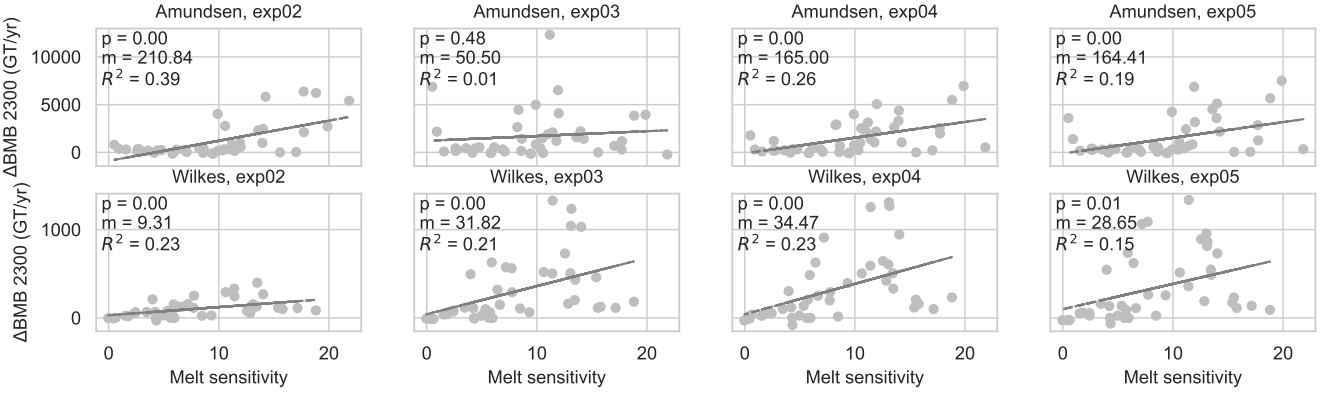

Figure 6. Melt sensitivity (MS) factor ($\mathrm{m\,yr^{-1}\,K^{-1}}$) versus the change in BMB ($\mathrm{Gt\,yr^{-1}}$) at 2300 for the Amundsen (top row) and Wilkes (bottom row) sectors. Colours indicate the MS factors for the sectors. Statistical significance is defined by Student's t-test when the p-value for the slope of the line of best fit is less than 0.05. The slope of the best fit line is reported (the m-value in the top left), along with the coefficient of determination (R^2 value).

than the previous case but lower than the mean minus half a standard deviation of the melt sensitivities; (iii) average sensitivity being within half a standard deviation of the mean sensitivities; (iv) large sensitivity being above this, but below one standard deviation from the mean; and (v) very large sensitivity being above the mean plus one standard deviation. The calving groups are those defined in Section 3.1.2 and summarised in Table 2.

Using 3-way ANOVA (Section 2.5), we analyse how much of the total variance in modelled basal mass balance ($\mathrm{Gt\,yr^{-1}}$) in each year of the projections can be explained by the variance in each single factor, and interactions between factors. Figure 7a shows the overall evolution of uncertainty, i.e., standard deviation, of basal mass balance relative to their 2015 value until 2300. The uncertainty increases from 500 $\mathrm{Gt\,yr^{-1}}$ in the first decade to 5000 $\mathrm{Gt\,yr^{-1}}$ by 2300. As indicated by the standard deviation explained by individual components in Fig. 7a, and the relative variance explained by each factor relative to the total variance, until about 2125, the melt sensitivity can explain up to 80% of the total variance in basal mass balance. After 2125, uncertainty in melt sensitivity becomes less important. The contribution from climate uncertainty reaches a maximum of 40%, but stays generally below 20%. From 2100, the calving group becomes relevant, and explains about 50% of the variance, most likely linked to their impact on ice shelf area, as described in Sections 3.1.2 and 3.1.3. Interactions between the groups do not play a significant role, except for initial climate-melt sensitivity interactions. Hence, as expected, the unexplained contribution to variance grows over time, and is about 60% by 2300.

To summarise, we find that the dominating factor for modelled uncertainty in BMB in the first 100 years is the variance in MS factors, while the dominating factor between 100 and 200 years is the variance in-between calving groups.

https://doi.org/10.5194/egusphere-2025-4069
Preprint. Discussion started: 14 October 2025

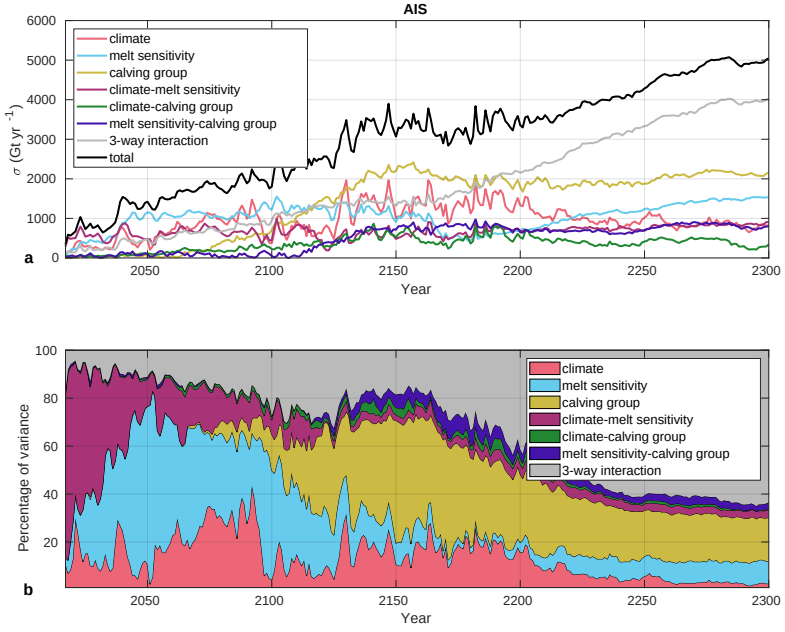

Figure 7. Sources of uncertainty in basal mass balance evolution ($\mathrm{Gt\ yr^{-1}}$). (a) Uncertainty from the climate model, melt sensitivity (combination of melt parameterisation and parameter tuning), and choices made about calving, and interactions between two or more components. (b) Relative variance of the different sources of uncertainty as a proportion of the total variance. We only consider the main submission of each modelling group in this analysis.

3.2 Relationship between melt and dynamic sea level

As a next step, we analyse the link between sub-shelf melting and dynamic sea level projections in the ISMIP6 Antarctic 2300 experiments. We start by analysing the link between the (pattern of) melt and dynamic ice loss (section 3.2.1), then introduce the dynamic ice loss sensitivity factor (section 3.2.2), and finally discuss the contribution of melt sensitivity and dynamic ice loss sensitivity factors to explaining overall uncertainty in the dynamic ice loss (section 3.2.3).

3.2.1 Linking melt and dynamic ice loss

We first establish that cumulative basal mass balance under the entire ice shelf is a good predictor for dynamic sea level rise. Across all sectors and experiments, we find a statistically significant (p<0.05) linear relationship between cumulative basal mass balance and dSLR in 2300 for all ice sheet models (Fig. 8). The average slope of this relationship is ∼0.4 for the Antarctic, with values ranging from 0.22 to 0.62 depending on the sector and experiment. This suggests that, on average, for every unit of mass lost due to basal melting beneath ice shelves, there is an additional 40% mass loss from the grounded ice. The Wilkes sector shows the strongest sensitivity of dSLR to cumulative basal melting across all experiments, while the Aurora

https://doi.org/10.5194/egusphere-2025-4069
Preprint. Discussion started: 14 October 2025

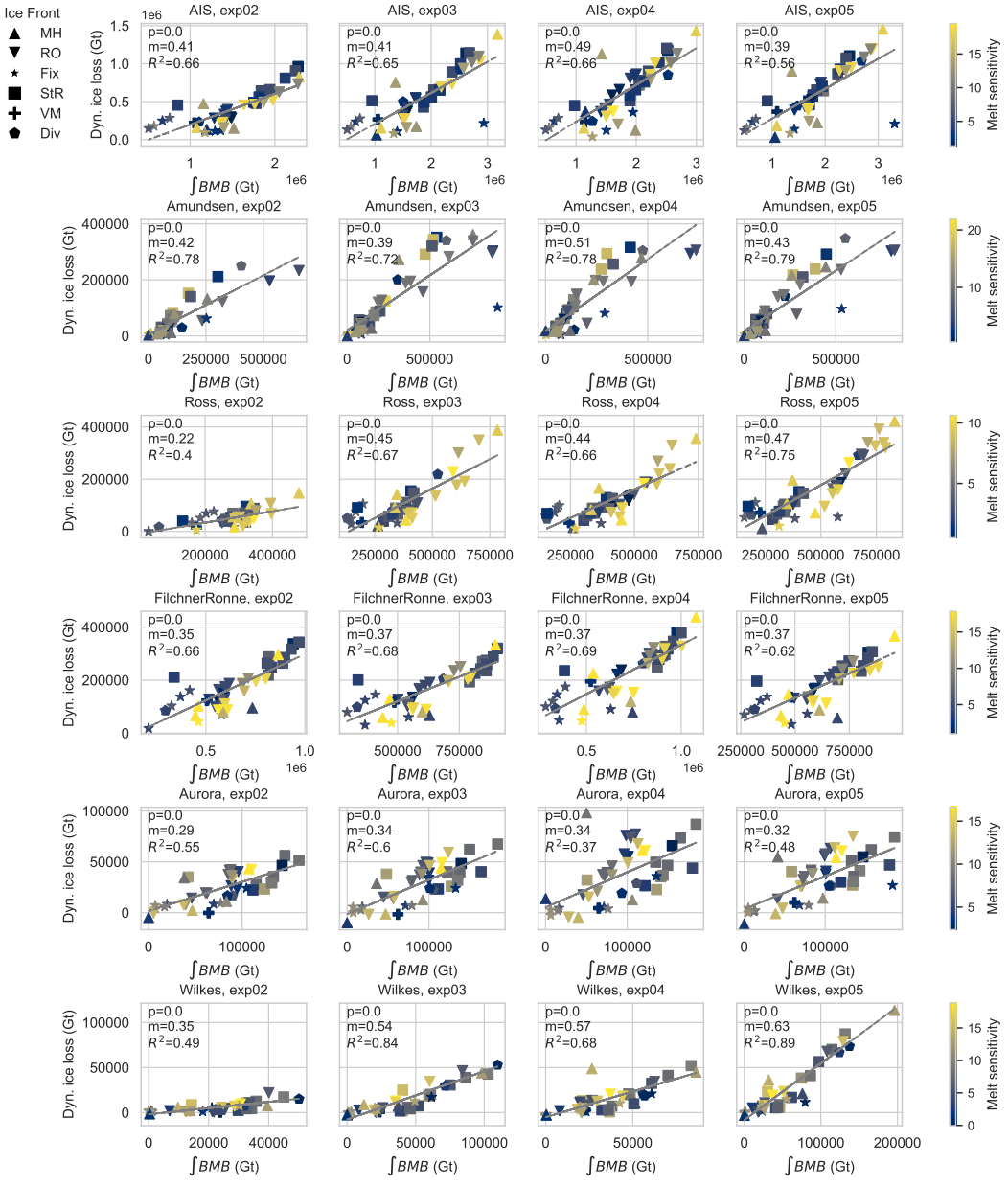

Figure 8. Dynamic sea level contribution (dSLR, Gt) vs. cumulative basal mass balance (Gt). The columns represent experiments exp02-exp05. Rows represent: aggregated Antarctic data, Amundsen, Ross and Filchner-Ronne Sectors, and the Aurora and Wilkes Subglacial Basins. The colours in each panel represent the MS factors ($\mathrm{myr}^{-1}\mathrm{K}^{-1}$); the markers represent the calving procedure (MH, RO, FF, SR, VM, Div). As per Fig. 6, statistical significance, slope, and coefficient of determination are reported in the top left of each panel (p, m, and R^2 values, respectively).

https://doi.org/10.5194/egusphere-2025-4069
Preprint. Discussion started: 14 October 2025

sector shows the weakest. We note that the magnitude of dSLR as a function of cumulative BMB varies as a function of the climate forcing experiment in some sectors, notably the Ross and Wilkes sectors where exp02 results in a substantially lower slope than the other experiments. This is linked to much lower cumulative BMB in 2300 in exp02, which indicates a potential nonlinearity in the dynamic response of the ice sheet to cumulative BMB. For the remaining sectors, there is a relatively smaller spread in the average slopes for each experiment.

When we categorise ice sheet model simulations based on ice front treatment (marker shape; Fig. 8) or MS (marker colour; Fig. 8), no clear pattern or consistent relationship with dSLR emerges for any sector. For the Amundsen and Wilkes sectors, which are less affected by calving (Section 3.1.3), we again find a statistically significant relationship between dSLR in 2300 and the melt sensitivity (Fig. S13), as for the Filchner-Ronne sector. However, the relationship is not statistically significant for the Ross and Aurora sectors.

We explore the relationship between the spatial pattern of basal melting and dSLR in Appendix C.

3.2.2 Dynamic ice loss sensitivity (DS) factor

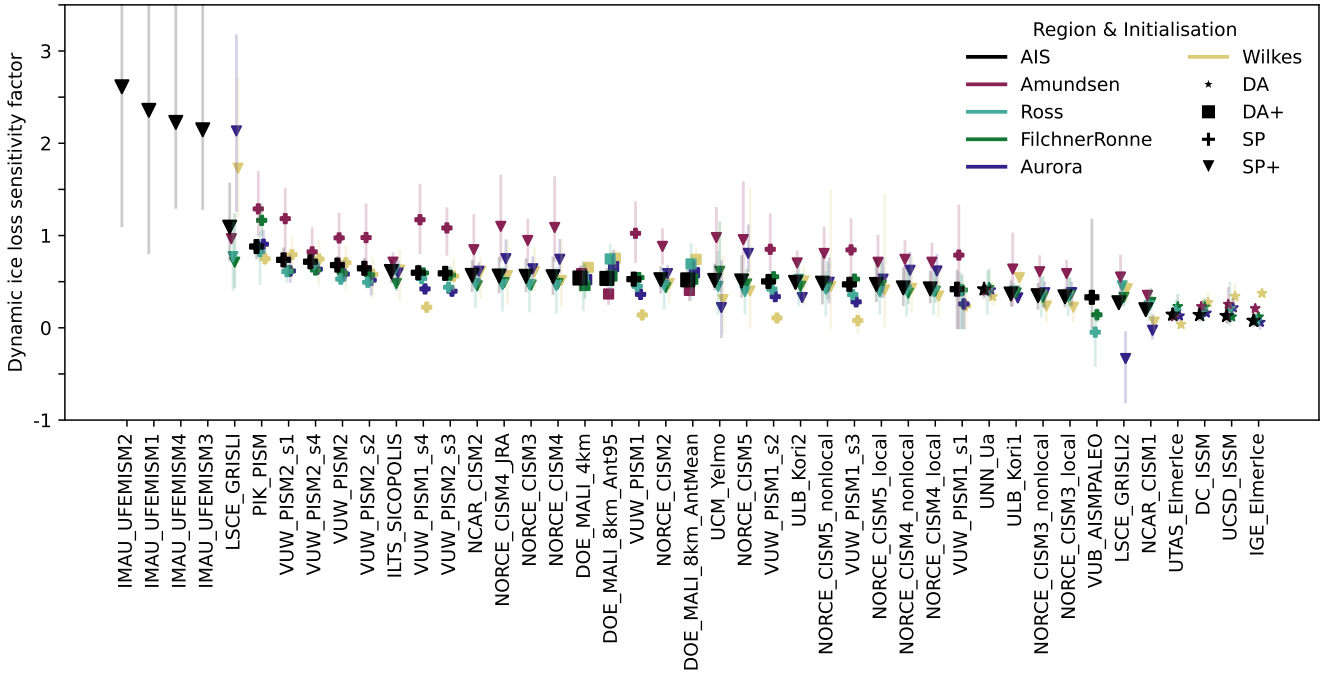

Figure 9. Dynamic ice loss sensitivity factor (unitless) for different ice sheet models and sectors. The markers represent the experiment-mean dynamic ice loss sensitivities determined for each ice sheet model and sector. The sectors and thin coloured lines are the same as in Fig. 3 The models on the x-axis are ordered by their Antarctic-wide dynamic ice loss sensitivity factor (in black), in descending order. Different markers denote the initialisation procedure used by each model: DA (data assimilation; star), DA+ (data assimilation with relaxation; square), SP (spin-up; plus), SP+ (spin-up with ice thickness target values; downwards triangle).

https://doi.org/10.5194/egusphere-2025-4069
Preprint. Discussion started: 14 October 2025

Similarly to the MS factor, the DS factor varies by up to an order of magnitude between the different ice sheet model simulations (Fig. 9), ranging from 0.1 to 2.6 for the mean Antarctic values (Table 2). A DS value of 1 means that on average 1 Gt of ice shelf melted at some point in the simulation will cause, through a loss of buttressing, a dynamic ice mass loss of 1 Gt from the grounded ice sheet. Values of 0.1 are roughly in line with the diagnostic response of more sensitive ice shelf areas (Reese et al., 2018b), while a value of 4 means that the sub-shelf melt is highly effective in driving grounded ice loss in the transient simulation, and causes ice losses larger than the direct melt. Most, but not all (29/39), model simulations have the highest DS factors in the Amundsen sector ranging from 0.1 to 1.3, indicating that this sector responds most sensitively to changes in basal melting. 6 of 39 model simulations have the highest DS value in the Wilkes sector, ranging from 0.0 to 1.7. The DS factors for the Amundsen and Aurora sectors (ranging from -0.3 to 2.1) vary by a similar magnitude to the whole Antarctic DS factor – noting that the Aurora has the largest differences between DS factors of all the sectors and that the smallest DS factor here is negative, indicating grounding line re-advance and negative sea level contribution in one ice sheet model. DS factors for the large ice shelves, Filchner-Ronne and Ross, range from 0.1 to 1.2 and 0.0 to 0.8, respectively. Note that for the VUB_AISMPALEO model, initial mass gain in the Amundsen, Aurora, and Wilkes sectors yields values for the DS factor well outside the expected range and high root mean square errors. This is due to the assumption of linearity between the cumulative BMB and dynamic ice loss in the derivation of the DS factor (Eq. 3), which is inappropriate in such scenarios. As such, we excluded the VUB_AISMPALEO values for these regions from Fig. 9. A similar result is found for the four IMAU_UFEMISM simulations for all sectors, so we report only the mean Antarctic values for these models.

As for the MS factor, there is no clear relationship between the DS factor and ice sheet model numerics or parameterisations, see Fig. S8. However, we find that members of a single ice sheet model ensemble have as large a spread in DS factors as different ice sheet models in some sectors, which indicates that both the choice of ice sheet model and the choice of model parameters can have an equally significant impact on the ice sheet response to ocean melting. In the Amundsen sector, there is a potential influence of initialisation on the DS factor, with all DA/DA+ simulations being grouped in the lowest 40% of DS factors; however, as for the MS factors in Section 3.1.1, given the relatively small number of simulations, we cannot establish statistical significance.

We investigate whether there is a relationship between the Antarctic MS and DS factors for different ice sheet model simulations (Fig. 10). As expected, there is no clear relationship between the two sensitivity factors: a high MS factor does not necessarily translate to a high DS. Rather, the magnitude of the DS factor depends on specific modelling choices that influence how the ice sheet responds to forcing, while the magnitude of the MS factor will depend on the melt parameterisation and related choices. Similarly, two DS factors of approximately the same magnitude do not require MS factors of approximately the same magnitude. Two case studies illustrate this. First, the two LSCE_GRISLI simulations have approximately the same MS factor (Table 2), but their DS factors vary by almost an order of magnitude, due to the choice of sub-grid melt parameterisation (Table 1). That is, LSCE_GRISLI uses a flotation criterion to determine how melt is applied on partially-floating cells, whereas LSCE_GRISLI2 specifies no melt on partially-floating cells. This choice naturally has an influence on how the ice sheet responds to melt, irrespective of the sensitivity of the melt rate to a given thermal forcing. Second, the three DOE simulations have MS factors that vary almost by a factor of two, but DS factors that are essentially the same (Table 2). Of the

https://doi.org/10.5194/egusphere-2025-4069
Preprint. Discussion started: 14 October 2025

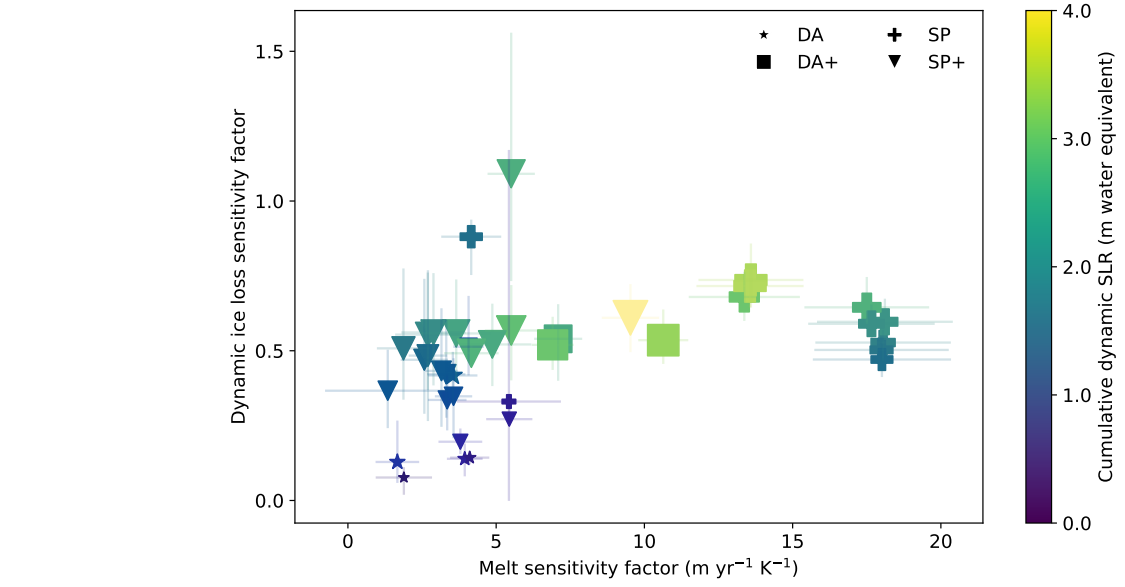

Figure 10. Melt sensitivity factor ($\mathrm{m\,yr^{-1}\,K^{-1}}$) versus dynamic ice loss sensitivity factor (unit-less). Marker colours and size reflect the cumulative dSLR (Gt) contributions at 2300. Vertical and horizontal error bars represent the range between the MS and DS factors for the four experiments exp02-exp05.

three ensemble members, the Ant95 simulation has the highest MS factor as it uses parameters tuned for melting in the 95th percentile (Jourdain et al., 2020). This comparison demonstrates that the MS and DS factors are independent and can be used to understand where the sensitivity of ice loss lies. In general, we find an approximate correspondence between the magnitude of the DS factor and the magnitude of sea level rise, as well as the magnitude of the MS factor and the magnitude of sea level rise in Fig. 10. Although not always true, in general a higher DS factor means higher dynamic ice loss, and a higher MS factor means higher dynamic ice loss. We explore this in more detail in terms of the uncertainty in projected dynamic sea level rise.

3.2.3 Uncertainties in dynamic sea level rise

We analyse the factors that contribute to uncertainty in the projected dynamic sea level rise. We use the categorical factors "climate"; "melt sensitivity" (MS), which represents the sensitivity of the melt parameterisation, its implementation and choice of parameters; and "dynamic sensitivity" (DS) which represents the ice sheet model, implementation, and parameter choices. As in Section 3.1.4, we represent the climate uncertainty by choice of climate forcing experiment, and the melt sensitivity is categorised into five bins. Similarly to the melt sensitivity, we also categorise the dynamic sensitivity into five bins based on mean and standard deviation DS among groups.

Figure 11 shows the total standard deviation in dSLR, which increases to just above 1 m sea-level equivalent by 2300. The uncertainty in dSLR can be largely explained by the uncertainty in the basal melting choices and the uncertainty in the ice sheet modelling choices. Prior to 2150, uncertainty in climate forcing is also relevant (about 15%), but the dominant source

https://doi.org/10.5194/egusphere-2025-4069
Preprint. Discussion started: 14 October 2025

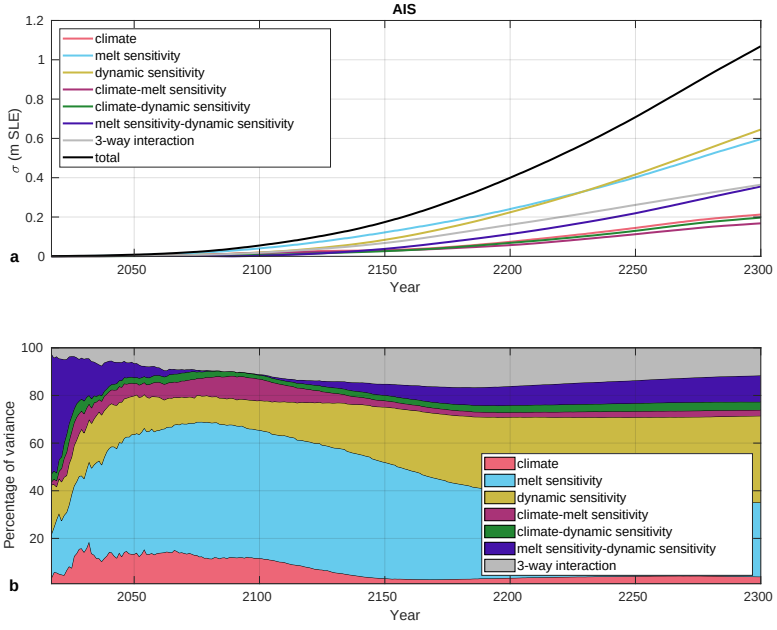

Figure 11. Sources of uncertainty in dynamic sea-level contribution (m sea level equivalent). (a) Uncertainty from the climate model, melt sensitivity (combination of melt parameterisation and parameter tuning), and dynamic ice loss sensitivity factor (representing choices made in the ice sheet model and their implementation), and interactions between two or more components. (b) Relative variance of the different sources of uncertainty as a proportion of the total variance. We only consider the main submissions of each modelling group here.

of uncertainty is the melt sensitivity (approx. 60%). Similar to the uncertainty in basal melt, we find a contribution from climate and melt sensitivity interactions, which is below 10% and potentially represents feedbacks between melting and ice shelf geometry. The dynamic sensitivity contributes about 10% of the entire uncertainty up to 2100, after which its contribution increases until it is about equal to the melt sensitivity by 2300. About 10% of the uncertainty stems from interactions between melt and dynamic sensitivities, and the other 10% represents the 3-way interaction of these three factors.

4 Discussion

This study investigates the role of ocean forcing in driving dynamic sea level rise in the ISMIP6 Antarctic 2300 experiments, including the relationship between ocean forcing and sub-shelf melting as well as the links between basal mass balance and dynamic ice loss. In this section, we discuss our results in the context of the role of the MS and DS factors in understanding the drivers of sea level rise (section 4.1) and how these vary in between sectors (section 4.2), and based on these, formulate recommendations for future studies (section 4.3).

https://doi.org/10.5194/egusphere-2025-4069
Preprint. Discussion started: 14 October 2025

4.1 Sensitivity in BMB and dynamic sea level projections

A key result from this study is the identification of MS and DS factors to predict ice sheet model behaviours, both in translating climate forcing into simulated sub-shelf melt rate, and in the dynamic response of the ice sheet to applied melt. The MS factor incorporates effects of the choice of melt parameterisation, its parameters, implementation, and realisation in the ice sheet model simulation. The DS incorporates effects of ice sheet model physics, parameters, implementation and realisation. We find that to a large extent, differences in these two sensitivity factors can explain uncertainties in projected dSLR.

Interestingly, the melt parameterisation alone is not a good predictor for the MS factor; rather, a combination of other aspects, such as choices made in the implementation and parameter value, influence the MS factor. An example of this is that for models that use quadratic local or non-local melt parameterisations it is not necessarily the case that the MS factor is higher in regions of high thermal forcing (e.g. the Amundsen Sea sector).

The MS factors derived from the ISMIP6 simulations can be compared with analogous values derived in previous studies. In the Amundsen Sea sector, the ISMIP6-derived MS factor values range from 0.55 to 21.85 $\mathrm{m\,yr^{-1}\,K^{-1}}$ (median 9.9 $\mathrm{m\,yr^{-1}\,K^{-1}}$). Observational data from this sector (Dutrieux et al., 2014; Jenkins et al., 2018) yield MS factors of 10-20 $\mathrm{m\,yr^{-1}\,K^{-1}}$ (Reese et al., 2023), which correspond well with the estimate of 16 $\mathrm{m\,yr^{-1}\,K^{-1}}$ from Payne et al. (2007) for the Pine Island Glacier ice shelf. Coupled ice sheet-ocean simulations of the Thwaites Glacier ice shelf (Seroussi et al., 2017), with a constant 0.5 K temperature increase applied to a present-day ocean thermal forcing field, indicate an initial MS factor of 16 $\mathrm{m\,yr^{-1}\,K^{-1}}$, although the MS factor in the coupled simulation decreases during the simulation, reaching a minimum value of 4.5 $\mathrm{m\,yr^{-1}\,K^{-1}}$ and having a mean of 9 $\mathrm{m\,yr^{-1}\,K^{-1}}$. For eight ice shelves of the Amundsen-Bellingshausen seas, the regional ocean projections at 2100 of Jourdain et al. (2022) indicate a sensitivity ranging from 10 to 20 $\mathrm{m\,yr^{-1}\,K^{-1}}$. Overall, these studies indicate that higher MS factor values are more plausible and/or consistent with observations and ocean model outputs for the Amundsen sector. This is due to generally high thermal forcing in the Amundsen sector, but can also include other effects like cavity geometry. Note that higher MS factors are not indicative of more accurate sea level projections given the multiple other factors that influence the ice sheet response to climate forcing, including the DS factor.

For the Filchner-Ronne sector, our MS factors range from 1.1 $\mathrm{m\,yr^{-1}\,K^{-1}}$ to 19.5 $\mathrm{m\,yr^{-1}\,K^{-1}}$. Using ocean model outputs from Naughten et al. (2022), Reese et al. (2023) identify MS factors between 0.7 and 1.5 $\mathrm{m\,yr^{-1}\,K^{-1}}$. By contrast, using plume theory, Jenkins (1991) finds an increase from 0.6 to 2.6 $\mathrm{m\,yr^{-1}}$ for a warming of 0.6 K in the Filchner-Ronne sector, which implies a higher MS factor of 3.3 $\mathrm{m\,yr^{-1}\,K^{-1}}$. Hellmer et al. (2012) report that a switch from cold to warm conditions in the same sector increases average melt rates from 0.2 to 4 $\mathrm{m\,yr^{-1}}$ for a warming of 2 K, which also implies a higher MS factor of 1.9 $\mathrm{m\,yr^{-1}\,K^{-1}}$, as also suggested by idealised studies (Gwyther et al., 2016). Finally, based on Comeau et al. (2022, Figs. 9d and S10), we can estimate an approximate MS factor of 3.5 $\mathrm{m\,yr^{-1}\,K^{-1}}$. In each of these previous studies the order of magnitude of the MS factor is comparable, indicating that for the Filchner-Ronne, lower MS factor values are more plausible.

The MS we define is a linear approximation to the melt response to ocean thermal forcing. Observational and idealised modelling studies indicate that the relationship between melt rates and ocean thermal driving might be quadratic (Holland et al., 2008; Jenkins et al., 2018) and we do not expect that a linear approximation will be able to capture rapid and high

https://doi.org/10.5194/egusphere-2025-4069
Preprint. Discussion started: 14 October 2025

magnitude changes in the melt response, e.g., as may be simulated using the quadratic melt parameterisation. The MS factor also represents a simplification of complex melt patterns and geometry feedbacks, including the effect of stratification to suppress or enhance turbulent mixing of heat to the ice-ocean interface (e.g., Galton-Fenzi et al., 2025), the effects of which cannot be clearly distinguished. Hence, higher thermal forcing does not automatically mean a higher MS factor. It would be worth examining the opportunities afforded by and limitations of the MS factor for classifying sub-shelf melt projections in more detail.

Our DS factors – ranging from 0.1 to 2.6 (median 0.5; unitless) – perform well at predicting simulated ice sheet model behaviour from cumulative BMB for the aggregated Antarctic data and on shorter timescales (decades to centuries). However, we found larger deviations between the simulated dSLR and that predicted using the DS factor when the rate of ice loss changed rapidly. This may be partly attributed to the simplified assumption of the linear relationship between melt rates and the ice sheet response, which is likely to break down when complex or nonlinear dynamics are at play. For example, previous studies have shown a nonlinear ice response to variable basal melt rates (Hoffman et al., 2019; McCormack et al., 2021; Reese et al., 2018a), amplified during periods of higher melt, where retreat is strongly controlled by the bed topography. In such conditions, our DS factor is likely to underestimate dSLR. We also expect that the linear relationship is not an appropriate approximation during periods of unstable grounding line retreat, e.g. associated with the marine ice sheet instability, where grounding line retreat rates are significantly higher than expected solely from the ice response to the forcing applied (e.g., Rosier et al., 2021; Seroussi et al., 2024). While it is possible to prescribe a nonlinear relationship between the cumulative BMB and dSLR to derive a more robust fit between the simulated and predicted dSLR, this comes at the risk of overfitting. On shorter timescales, including over the satellite era where sub-shelf melt rate and dynamic ice loss datasets are available (e.g., Adusumilli et al., 2020; Davison et al., 2023; Otosaka et al., 2023; Paolo et al., 2023), our linear prescription for the DS factor is likely to be robust. This affords opportunities to use the DS factor calculated using observations as a metric to assess or calibrate modelled outputs, including e.g., the magnitude of and variability in basal melt rates from an ocean model.

We are not able to establish statistical significance between the MS or DS factors and the underlying numerics, initialisation and calving procedures, mesh resolution, or melt rate parameterisation due to a low sample size. Importantly, this likely indicates that a combination of factors determines the sensitivity of the basal melt rate response to thermal forcing and ice sheet response to basal melting — rather than one sole factor – and we were unable to isolate the influences of different factors. This result is not surprising. For example, models that use spin-up initialisations often rely on coarser resolution meshes due to the computational expense of the longer simulation times, which means that the influences of the initialisation procedure and resolution cannot necessarily be easily distinguished (Seroussi et al., 2019). Certain choices for numerical and physical schemes do appear to make a difference in influencing the magnitude of the MS or DS factors in certain sectors, which was particularly evident when there was a larger number of ensemble members of the same ice sheet model, as discussed below.

Other studies have assessed the influence of ice sheet model choices on basal melting and dSLR. Multiple studies have shown that a mesh resolution of at least 1 km is required to constrain sea level projections from Antarctica, both for short-term change under projected emission scenarios (c.f., Castleman et al., 2022; Seroussi et al., 2017) and low probability, high-tail scenarios under more extreme warming (Williams et al., 2025). Resolution also influences grounding line retreat via the numerical

https://doi.org/10.5194/egusphere-2025-4069
Preprint. Discussion started: 14 October 2025

treatment of basal melting and friction in the grounding zone (Gladstone et al., 2017; Seroussi and Morlighem, 2018; Wang et al., 2024; Zhao et al., 2022). For example, in a study using an idealised marine ice sheet domain (Seroussi and Morlighem, 2018), application of basal melting at the sub-element scale and no melt applied on partially floating elements both generally result in lower sensitivity in grounding line retreat rates than when melt is applied on partially floating elements; however all three numerical treatments of melt converge at finer mesh resolution. However, this was found not to be the case for other ice sheet models (Leguy et al., 2021). Previous studies have also evaluated different melt rate parameterisations in ice sheet models (e.g., Berends et al., 2023; Burgard et al., 2022; Favier et al., 2019), making recommendations for the choice of melt rate parameterisations based on the fidelity to modelled melt rates.

While these studies provide a suite of recommendations towards model choices for producing accurate sea level projections, uncertainties in parameters, initialisation, models, and how the ice sheet responds to chaotic atmosphere and ocean dynamics remain a challenge (Aschwanden et al., 2021; Hill et al., 2021; Hoffman et al., 2019; Robel et al., 2022). The use of emulators alongside large ice sheet model ensembles (e.g., Berdahl et al., 2021; Edwards et al., 2021; Van Katwyk et al., 2023) provides a means to quantify uncertainty through constraining the sea level probability distribution from a range of different model choices. Another means is via observationally-constrained ensembles (e.g., Coulon et al., 2024). Here, our MS and DS factors could prove useful model tuning factors to work towards this aim.

4.2 Drivers of uncertainty in melt rates and dynamic ice loss

We find that uncertainties in integrated, continent-wide basal mass balance are initially dominated by the uncertainty in melt sensitivity, especially until 2150. After 2100, the choice of calving schemes becomes more important, where we distinguish between strong calving (here encompassing model simulations that determine calving based on strain rates, ice shelf thickness calving criterion applies for ice shelf thicknesses higher than 200 m, von Mises stresses) and weak calving (model simulations that determine calving based on the current ice shelf extent, ice shelf thickness criterion applies for ice shelf thickness at or below 50 m, divergence and accumulated strain). The importance of uncertainty in the climate forcing peaks at 40%, but generally remains below 20%.

When analysing the different sectors, we found that the evolution of basal mass balance for the Filchner-Ronne and Ross sectors in the ISMIP6 Antarctic 2300 simulations is tied to both thermal forcing and calving. In these sectors with large ice shelves, the calving group is a strong predictor of ice shelf area change and the overall BMB. This is in contrast to sectors with small ice shelves: in the Amundsen sector, we found that melting is the dominant factor controlling the overall ice sheet behaviour simulated, with the MS factor being a clear predictor of the simulated BMB (and dSLR) to 2300. This is because we found no major calving-driven ice shelf area change in the Amundsen Sea as we found in the large Filchner-Ronne or Ross ice shelves where the calving treatment in the model simulation influences basal mass balance projections substantially. Similar to the Amundsen sector, melting is the key factor determining the evolution of the Wilkes sector, and there is no major influence of calving treatment on melt rate projections. The evolution of basal mass balance in the Aurora sector is more strongly tied to the calving group than the MS factor. However, given that the steep and narrow bed topography of the Vanderford Trench

https://doi.org/10.5194/egusphere-2025-4069
Preprint. Discussion started: 14 October 2025

is the primary pathway for warm water driving melt in this sector, if model resolution is too coarse to resolve this feature, we might expect that simulated melt is not well captured relative to observed conditions.

We found that up to 80% of the uncertainty in the projected dynamic sea level contribution can be explained by uncertainties in the melt sensitivity and the dynamic sensitivity. Uncertainties in the climate forcing explain around 15% of the dynamic sea level uncertainty until 2100, after which their importance decreases. This is broadly in line with the influence of climate forcing found by Seroussi et al. (2024), who report a continued influence of 15% until 2300. The difference could be linked to the uncertainties in surface mass balance evolution, which is considered in the initial ISMIP6 Antarctic 2300 analysis, and which we exclude here. Seroussi et al. (2024) also analyse ice shelf collapse, which we exclude here. Moreover, they found that 50-95% of uncertainty in the full sea level contribution (including changes in the SMB) is explained by uncertainties relating to the ice sheet modelling choices. This would include all choices made, and we here disentangle those by introducing the MS and DS factors into choices around the sub-shelf melting and dynamic uncertainty in the model simulation (note that part of the MS will also be linked to the interactions between climate and modelling choices in Seroussi et al. (2024) as discussed further in Seroussi et al. (2023)). We represent both by simple sensitivity factors, and find that these can explain up to 80% of the uncertainty in dynamic ice loss. This indicates that the MS and DS factors and their spread are useful indicators to understand uncertainties in Antarctic Ice Sheet projections.

For the Amundsen, Wilkes, and Aurora sectors, the MS and DS factors show a large spread across ice sheet model simulations. That these marine basins have such a broad spread of sensitivities is a concern, which has implications for the usefulness of probabilistic estimates of projected sea level rise in these sectors, including from emulation, if there is considerable ambiguity in the magnitude and timing, and potentially even sign, of ice loss. These issues highlight the need for further process-based and high-resolution regional ensembles to provide specific recommendations on how to treat these sectors – including in choice of parameterisations, resolution, physical schemes, and numerics – in continental-scale models. The Wilkes sector also generally shows the strongest sensitivity in the dSLR response to cumulative basal mass balance at 2300 compared with all other sectors (for all but the exp02 experiment where the Amundsen is the most sensitive), which may be linked to its sensitivity to the sub-grid melt parameterisation, as also found in Wang et al. (2024). Interestingly, members of a single ice sheet modelling group ensemble generally have as large a spread in Wilkes DS factors as different ice sheet model simulations, which is not necessarily the case for other sectors.

We considered the relative contributions of shelf-wide melt (Joughin et al., 2021) versus melt at the grounding line (Arthern and Williams, 2017; Robel et al., 2022) in impacting dSLR (appendix C). We found a statistically significant relationship between melt at the grounding line and dSLR. However, our analysis also indicated that melt at deep and shallow ocean levels contributes to dSLR, making it impossible to pinpoint whether specific depth ranges were most critical to ice loss from the simulations analysed here. Resolving this question requires targeted experiments, such as artificially increasing melt within specific depth ranges and assessing the resulting dSLR.

https://doi.org/10.5194/egusphere-2025-4069
Preprint. Discussion started: 14 October 2025

4.3 Key recommendations

Based on our analysis, we summarise some key suggestions that will facilitate improved understanding of the drivers of future ice loss, including as simulated by ISMIP7.

1. Further exploration of MS and DS factors. We find that the spread in the MS and DS factors can be used to explain a large part of the overall uncertainty in dynamic ice loss. However, the target ranges of values for these factors are generally poorly constrained at continental and regional scales. Better constraining MS and DS factors using observational data, theory, paleo-climate proxies, and high resolution coupled ice sheet-ocean models would be valuable for calibration of dSLR to reduce uncertainties (Aschwanden et al., 2021), or to serve as targets for modellers to constrain model parameters or parameterisations in their initialisation, or to test their model sensitivity. As discussed in Section 4.1, these factors were derived using linear regression, which may neglect important nonlinearities, including, e.g., behaviours associated with instabilities or regime shifts. Alternate definitions for the MS and DS factors could be explored that are more versatile and complex across different simulated ice sheet behaviours.

2. Expanding understanding of projections via new sensitivity factors. Further processes could be analysed using similar sensitivity factor approaches to the one we used here for the MS and DS factors. For example, given that we find an influence of calving on ice loss timing, we suggest that a calving sensitivity factor, linking calving fluxes to ice loss, could be derived. Alternatively, a buttressing sensitivity factor that combines MS and calving sensitivity factors could be explored. Furthermore, we considered only the dynamic ice loss contributions to total sea level rise, removing the role of surface mass balance changes. However, surface mass balance changes could contribute to ice loss in some sectors over the coming decades to centuries (Gilbert and Kittel, 2021; Coulon et al., 2024; Jourdain et al., 2025), and the response to surface mass balance changes could also be assessed individually (e.g., Winkelmann et al., 2012) and jointly. Importantly, the MS and DS factors that we analysed in this study do not include important processes that are not currently modelled, such as damage evolution (e.g., Kachuck et al., 2022; Ranganathan et al., 2024), which has implications for ice shelf buttressing, hydrofracture and collapse, and hence could play a pivotal role in the evolution of the Antarctic Ice Sheet over the coming centuries.

3. Model tuning using sensitivity factors. The use of MS and DS factors as we have derived here could be valuable in calibrating short timescale (decades to centuries) simulated ice sheet behaviours against observed behaviours. For example, when tuning parameters for a melt parameterisation, we suggest modellers consider not only present-day melt rates (Jourdain et al., 2020), but also the sensitivity of melt rates to ocean forcing (MS factor) on a regional basis, and select parameters in their parameterisation accordingly. Furthermore, ice sheet models might be initialised or parameterised through matching the DS factor calculated from the observational record of discharge to a simulated DS factor over the same period.

4. Development of calving procedures. We found that calving played a significant role in determining the timing of ice shelf area loss, consistent with other community efforts and previous studies. Few studies have investigated how calving

https://doi.org/10.5194/egusphere-2025-4069
Preprint. Discussion started: 14 October 2025

parameterisations capture observed calving in Antarctica (Wilner et al., 2023) and further developments of calving parameterisations and advice around parameter values are needed. As mentioned under point 2, these parameterisations should incorporate important processes like damage evolution that are not typically explicitly represented. Projects like CalvingMIP can help foster such developments (Jordan and the CalvingMIP team, 2025).

5. Expanding model ensembles. For some sectors and ice sheet models, we found as much variation in the DS and MS factors between members of a single ice sheet modelling group ensemble as the variations across different ice sheet models. However, given limited sample sizes we could not necessarily use differences between ensemble members to say anything conclusive about the factors that influence melt or ice loss sensitivity, or to attribute uncertainties between different ice sheet models to any specific driver. Larger, observationally-calibrated (Aschwanden et al., 2021; Aschwanden and Brinkerhoff, 2022; Coulon et al., 2024) ensembles for each ice sheet model, in conjunction with emulation (e.g., Berdahl et al., 2021; Edwards et al., 2021; Van Katwyk et al., 2023), would be of immense benefit in addressing this limitation. In particular, we recommend ensembles that can disentangle, and calculate uncertainties associated with (Aschwanden and Brinkerhoff, 2022): the influence of the melt rate parameterisation; initialisation procedure, including the influence of any potential model drift; the calving procedure; and the role of shelf-wide melt versus melt close to the grounding line. In recommending this, we recognise that providing ice sheet model outputs for ISMIP and other model intercomparison projects is a huge undertaking, often provided as a community service, and that the resources required for larger ensembles may be prohibitive, hence such studies could be conducted with individual models. When constructing an emulator, we suggest it may be beneficial to include the MS and DS as probabilistic inputs covering the range of these sensitivities for a specific study domain. The emulator can then be run for the full distribution of our sensitivity factors, which allows us to propagate the associated uncertainty and yield, for example, a probabilistic sea level rise estimate with uncertainties rooted in MS and DS. The exact implementation of this will depend on the specific type of emulator, for example when using neural networks this can be a conditional input which is commonly used in neural network architectures (e.g., Mirza and Osindero, 2014; Garnelo et al., 2018).

5 Conclusions

Our study aims to understand the role of sub-shelf melting in introducing uncertainty in dynamic ice loss projections from ISMIP6 Antarctic 2300. To address this, we introduced two quantities: (1) a melt sensitivity factor, which translates changes in ocean thermal forcing to changes in melting via a linear approximation; and (2) a dynamic ice loss sensitivity factor, which translates cumulative sub-shelf melt to dynamic ice loss via a linear approximation. These sensitivity factors together explain approximately 75% of the variance in the dynamic sea level projections in 2300. Further continent-wide and regional investigations of these sensitivity factors from observational data, theory, paleo-climate data, and high resolution modelling, as well as a widening of the sensitivity analysis undertaken here to other ice sheet processes (e.g., calving where we found a large influence of modelling choices on integrated melt), will be valuable for calibrating and constraining ice sheet model parameters, and ultimately reducing uncertainty in sea level rise projections.

https://doi.org/10.5194/egusphere-2025-4069
Preprint. Discussion started: 14 October 2025

Code and data availability. Underlying data is available from Seroussi et al. (2024). Processed data and analysis scripts will be uploaded on a repository, e.g., zenodo, for publication.

Appendix A: Quality Control

We provide a series of jupyter notebooks, containing visualizations of some useful variables for each of the ISMIP6 models. The purpose of these notebooks is to provide an overview of the data; make an initial assessment of any issues with the individual model data as a precursor to making adjustments or corrections (see Appendix B); and to provide a tool to reduce barriers to accessing the datasets. The notebooks can be adapted and modified for anyone wanting to explore the data in further detail.

For each model, the notebooks provide visualisations for the control simulation (constant climate forcing) and exp05 (one of the four high-emission scenario experiments). The scripts initially check start and end dates of the model simulation and the timestep, all of which differ slightly between models. Next, we check the grid resolution that the data are provided at, noting that this may be different to the native resolution used for the model simulation.

The notebooks visualise the floating area and ice thickness at the start, middle and end of the simulation, and the total floating area over time. Models using the level set method to define the calving front (e.g., ISSM) will flag areas of ocean as floating ice. If needed, the true area of floating ice could be recalculated by finding floating regions with ice over a given thickness threshold. One notable feature is the repetitive spikes in the floating area in VUW_PISM1 control simulations, which are likely related to the parameterisation of subgrid basal melt at the grounding line as they do not appear in VUW-PISM2 experiments. We also include a check to find any areas of the floating mask where the ice shelf draft is found to be negative (i.e., the ice base is above sea level), which occurs for DOE_MALI, DC_ISSM, and UNN_Úa simulations.

Finally, we visualise the basal mass balance: plotting the minimum and maximum values; visualising basal mass balance in West Antarctica; and calculating the continent-wide total over time. The floating and total basal mass balance are plotted separately, visualising which models include basal mass balance on grounded ice.

Appendix B: Adjustments and corrections to model outputs

During our analysis, we identified inconsistencies and missing data in the output of several ice sheet models. For completeness, we list the modifications and adjustments made to the original submissions for the following models:

- IMAU_UFEMISM (all ensemble members): The mask data for floating ice (sftflf) comprised the total ice mask (sftgif) rather than the floating mask. We recalculated the floating mask based on a flotation criterion and ice thickness data (lithk), creating a new floating ice mask. This mask was updated to include all floating grid cells with a base above the underlying bedrock (topg). Additionally, we generated ice base fields by subtracting ice thickness from the ice surface (orog) as these files were missing but necessary for creating the thermal forcing files. The new floating ice mask will

https://doi.org/10.5194/egusphere-2025-4069
Preprint. Discussion started: 14 October 2025

also impact time series calculations of total basal melting and floating ice shelf area. These (iarefl, shelfmelt) were recalculated for IMAU_UFEMISM and differ to the data of Seroussi et al. (2024).

- UCM_YELMO: The ice base files did not correctly represent the base of the floating ice. To address this, we generated a new ice base field by subtracting the ice thickness (lithk) from the ice surface (orog).
- Ice mask handling (all model submissions): We set ice mask values below 0 to 0 and values above 1 to 1 for subsequent processing and to ensure consistency with Seroussi et al. (2024). All aggregated values were calculated using the same procedure described in Seroussi et al. (2024), namely by multiplying them with the ice mask m_ice (and floating mask m_fl if required), resolution grid area res_a and the area distortion scaling factor scalefac before being summed:

$$\text{shelfarea}(t) = \sum(\text{m\_fl}(t) \cdot \text{m\_ice}(t) \cdot \text{scalefac} \cdot \text{res\_a})$$

Appendix C: Influence of the spatial pattern of melting

We here analyse the spatial patterns of melting, i.e., melting close to the grounding line or at different depth, and how the influence the dynamic sea level contribution.

C1 Method: Variables defined at depth bins

To investigate the basal melt at different depths, we generated a dataset of basal melt for each sector, binned by depth and time (z,t). We employ 60-m deep depth bins, from the surface (0 m) to a maximum depth of -1770 m, similar to the depth bins on which the thermal forcing for each climate model experiment is provided. For each depth bin, we calculated the basal melt rate and total shelf area; dividing the melt rate by the area yielded the average basal melting in each bin.

C2 Method: Grounding line variables

To investigate the impact of melt close to the grounding line, we developed a dataset focused on melt near the grounding line. To achieve this, we tracked the grounding line position at each time step by identifying each grounded cell directly adjacent to the floating ice mask. We evaluated the melt rate in the adjacent floating cells, considering those within 32 km from the grounding line. Cells with a floating mask value greater than zero were included, allowing for the consideration of partially floating cells. We consider the four cells sharing vertices ("nearest four neighbours") with each grounding line cell, if they are floating. We then consider the neighbours of all detected cells given the variation in model resolution – from 4 km to 32 km – that requires an adjustment in the number of iterations for neighbour detection. Specifically, we divided the 32 km corridor length by the model's spatial resolution to determine the required iterations. For example, for models with a 32 km resolution, the neighbour detection was performed once, whereas in models with a 4 km resolution, it was performed eight times. This approach ensured consistency across different model resolutions. After identifying the relevant cells, we aggregated the melt rate data for each sector.

https://doi.org/10.5194/egusphere-2025-4069
Preprint. Discussion started: 14 October 2025

C3 Result: Grounding line melt

We first examine whether a relationship exists between dSLR and cumulative melt near the grounding line. As for the relationship between total cumulative basal mass balance and dSLR in 2300, we find a statistically significant relationship between the cumulative basal mass balance calculated within a 32 km corridor of the grounding line (Section C2) and dSLR (supplementary Fig. S14). In general, the R^2 values for the relationship between the total cumulative basal mass balance and dSLR are higher than those for the cumulative melt near the grounding line, indicating that the total cumulative basal mass balance is a better predictor of dSLR. Whether a 32 km corridor is the most appropriate distance to define a grounding line melt variable cannot be assessed for the current results; 32 km is the minimum distance that allows us to include all ice sheet model simulations given that the resolution of outputs ranges from 4 to 32 km. We hence conclude that grounding line melt is also indicative of dynamic ice loss, which is not surprising as the grounding line melt is included in the total melt.

C4 Result: Melting at depth levels

Melting near the grounding line is sometimes equated with melting at deeper ocean levels or within specific depth ranges. To investigate where at depth melt has the greatest impact on dynamic sea level changes, we investigated the relationship between cumulative basal melt in different depth ranges and dSLR. We calculated the cumulative melt at the deepest level in the dataset (1800 m) and progressively summed melt from shallower levels up to the surface. To compare the significance of different depth ranges, we normalised the standard error by the standard error from the full-depth analysis, creating a relative standard error (relSE). The results are summarised in Fig. A1.

Starting from the deepest levels (1800 m below sea level) and summing melt upward for each model until 2300, we find a statistically significant relationship ($p < 0.05$) between cumulative basal melt at the lowest depth range and dSLR for the Antarctic, Filchner-Ronne and Amundsen sectors, and the Wilkes Subglacial Basin. In contrast, for the Aurora Subglacial Basin and Ross Shelf, the p-values only dropped below 0.05 after including melt from shallower ranges: between 1800 and 1000 m below sea level for the Aurora Subglacial Basin. Adding melt from increasingly shallower depths improved the relationship, with p-values nearing zero around 300 m. Similarly, the relSE decreased as more depth levels were included. However, we note that this result may be influenced by differences in the ice shelf drafts simulated by the different ice sheet models, where outliers in the ice shelf draft could substantially impact whether or not statistical significance was established.

Row 3 highlights the fraction of ISMs with no basal melt at specific depth ranges, showing that this fraction decreases as more depth levels are included. Rows 4 and 5 reveal that the correlation and fraction of cumulative melt from a given depth range relative to total shelf melt improve when including shallower depths, exceeding 0.5 near 300 m. Cumulative melt between 1800 m and 1000 m is sufficient to establish a statistically significant relationship with dSLR by 2300, and melt from 1800 m to approximately 300 m accounts for ∼50% of the total basal melt beneath the shelf.

Reversing the analysis – starting from the surface and progressively adding deeper levels – produced similar results (Fig. S13), with cumulative melt from the surface to ∼300 m explaining ∼50% of the total basal melt. That is, in both cases we can find statistically significant relationships between melt and dSLR within certain depth ranges, although the exact depth range varies

https://doi.org/10.5194/egusphere-2025-4069
Preprint. Discussion started: 14 October 2025

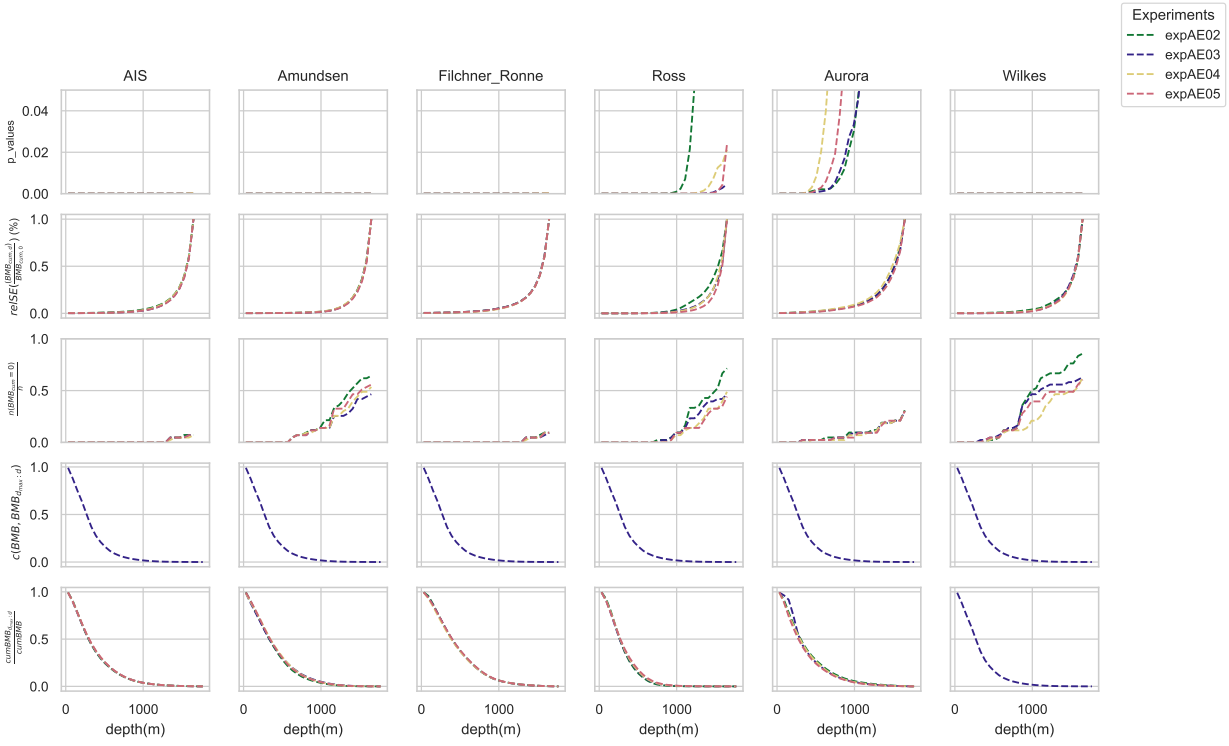

Figure A1. Relationship between melt within different depth ranges and dSLR. The top row shows the change in p-values between melt across depth ranges and dSLR, for the sectors of interest (column), and experiments (colours). The second row shows the change in relative standard error (relSE) between the melt across depth ranges and dSLR. The third row indicates the fraction of ice sheet models with zero basal melt within a given depth range (which could be indicative of no ice shelf draft at that depth), normalised by the total number of ice sheet models (a value of 1 means no melting across all models, and 0 means melting in all models). The final two rows show the average correlation between the melt across depth ranges and dSLR and the fraction of cumulative melt from a specific depth range to total basal melt beneath the entire shelf.

for different model simulations. Irrespective of the depth ranges chosen, as long as the cumulative melt is of a sufficiently high magnitude, we can obtain a significant relationship. Thus, we cannot determine whether melting at depth or the surface is relatively more important, nor whether the results are biased (e.g., by the ice shelf area present in each depth range); answering this question would require individual targeted experiments.

740 *Author contributions.* The study was designed by Johanna Beckmann, Ronja Reese, and Felicity McCormack. The work was kick-started during a hackathon organised by Johanna Beckmann, Ronja Reese, Felicity McCormack with participants Sue Cook, Lawrence Bird, David Gwyther, Daniel Richards, Matthias Scheiter, and Yu Wang. The quality control was led by Sue Cook, supported by Matthias Scheiter and

https://doi.org/10.5194/egusphere-2025-4069
Preprint. Discussion started: 14 October 2025

Yu Wang, while initial data processing was developed by Johanna Beckmann, Ronja Reese, Felicity McCormack, Lawrence Bird, David Gwyther, and Daniel Richards. Post-hackathon analysis was conducted and figures produced by Johanna Beckmann, Felicity McCormack, and Ronja Reese. Hélène Seroussi supported the development with advice, as the analysed data was gathered for the ISMIP6 AIS 2300 study led by HS with model contributions provided by all other authors. The manuscript was written by Johanna Beckmann, Ronja Reese, and Felicity McCormack, advised by all co-authors.

Competing interests. Some authors are members of the editorial board of the Cryosphere.

Acknowledgements. We thank the Climate and Cryosphere (CliC) effort, which provided support for ISMIP6 through sponsoring of workshops, hosting the ISMIP6 website and wiki, and promoted ISMIP6. We acknowledge the World Climate Research Programme, which, through its Working Group on Coupled Modelling, coordinated and promoted CMIP5 and CMIP6. We thank the climate modeling groups for producing and making available their model output, the Earth System Grid Federation (ESGF) for archiving the CMIP data and providing access, the University at Buffalo for ISMIP6 data distribution and upload, and the multiple funding agencies who support CMIP5 and CMIP6 and ESGF. We thank the ISMIP6 steering committee, the ISMIP6 model selection group and ISMIP6 dataset preparation group for their continuous engagement in defining ISMIP6. This is ISMIP6 contribution No 36. Johanna Beckmann, Felicity McCormack, and Lawrence Bird were supported under the Australian Research Council (ARC) Special Research Initiative (SRI) Securing Antarctica's Environmental Future (SR200100005). Felicity McCormack was supported under an ARC Discovery Early Career Research Award (DE210101433). David Gwyther was supported by an ARC Discovery Project (DP22010252). Sue Cook and Yu Wang received grant funding from the Australian Government as part of the Antarctic Science Collaboration Initiative program. Matthias Scheiter was supported by the ARC SRI Australian Centre for Excellence in Antarctic Science (SR200100008). Ronja Reese was supported by the UKRI Natural Environment Research Council [grant numbers NE/Y001451/1, NE/Z503344/1]. The Monash University Faculty of Science Uplift Grant supported Ronja Reese's visit to Monash and contributed to workshop costs, including travel and costs associated with hosting the ISMIP6 hackathon at Monash University in March 2024 involving Joanna Beckmann, Ronja Reese, Felicity McCormack, Lawrence Bird, Daniel Richards, David Gwyther, Sue Cook, Yu Wang, and Matthias Scheiter. Pierre Mathiot and Nicolas C. Jourdain received funding from Agence Nationale de la Recherche - France 2030 as part of the PEPR TRACCS programme under grant number ANR-22-EXTR-0010 (ISClim). Justine Caillet, Fabien Gillet-Chaulet and Nicolas C. Jourdain were funded by Agence Nationale de la Recherche under Grant numbers ANR-19-CE01-0015 (EIS) and ANR-22-CE01-0014 (AIAI). Petra Langebroek, David M. Chandler, Nicolas C. Jourdain, Julius Garbe, Ronja Reese, Hilmar Gudmundsson and Pierre Mathiot received funded from the European Union's Horizon 2020 Research and Innovation Programme under Grant Agreement No. 820575 (TiPACCs). Justine Caillet, Violaine Coulon, Jean-Baptiste Barre, Constantijn J. Berends, Fabien Gillet-Chaulet, Hilmer Gudmundsson, Heiko Goelzer, Phillipe Huybrechts, Jonas Van Breedam, Nicolas C. Jourdain, Ann Kristin Klose, Frank Pattyn and Anthony J. Payne received funding from the European Union's Horizon 2020 Research and Innovation Programme under Grant Agreement No. 869304 (PROTECT). Torsten Albrecht, Violaine Coulon, Nicolas C. Jourdain and Frank Pattyn were supported by OCEAN:ICE, which is co-funded by the European Union through the Horizon Europe Funding Programme for research and innovation under grant agreement number 101060452 and by UK Research and Innovation. Helene Seroussi and Mathieu Morlighem acknowledge support from the Novo Nordisk Foundation under the Challenge Programme 2023 (Grant number NNF23OC00807040) and from NASA Cryospheric Science Program (Grant number 80NSSC22K0383). Jorge Alvarez-Solas was supported by the Spanish Ministry of Science and Innovation (project CCRYTICAS, grant no.

https://doi.org/10.5194/egusphere-2025-4069
Preprint. Discussion started: 14 October 2025

PID2022-142800OB-I00). Heiko Goelzer has received funding from the Research Council of Norway under project 343397 (CLIM2Ant). Petra Langebroek was also supported by the Research Council of Norway through the Centre of Excellence iC3 (project number 332635). Resources were provided by Sigma2 - the National Infrastructure for High Performance Computing and Data Storage in Norway through projects NN8085K, NN11016K, NS8085K, NS11016K and NS5011K. Chen Zhao, Yu Wang, and Ben K. Galton-Fenzi received grant funding from the Australian Government as part of the Antarctic Science Collaboration Initiative program (ASCI000002). Chen Zhao is funded under an ARC Discovery Early Career Researcher Award (DE240100267). Rupert Gladstone was supported by the Research Council of Finland (grant numbers 322430 and 355572), and by the Finnish Ministry of Education and Culture and CSC-IT Center for Science (Decision diary number OKM/10/524/2022). Thomas Zwinger was supported by the Research Council of Finland (grant number 322978). Ralf Greve was supported by Japan Society for the Promotion of Science (JSPS) KAKENHI Grant JP16H02224, JP17H06104, and JP17H06323. Gunter Leguy and William Lipscomb are supported by the NSF National Center for Atmospheric Research (NCAR), which is a major facility sponsored by the U.S. National Science Foundation under Cooperative Agreement No. 1852977. Simulations for CISM were supported by the high performance computing Derecho system (doi:10.5065/qx9a-pg09) and computing resources provided by the Climate Simulation Laboratory at NSF NCAR's Computational and Information Systems Laboratory (CISL). Marisa Montoya was supported by the Spanish Ministry of Science and Innovation (project MARINE, grant no. PID2020-117768RB-I00). Tyler Pelle was supported by the NASA Cryosphere program under grants 80NSSC22K0387 and 80NSSC20K1134, NSF grant OPP-2114454, and the Cecil H. and Ida M. Green Foundation for Earth Sciences at the Institute of Geophysics and Planetary Physics at the Scripps Institution of Oceanography. Nicholas R. Golledge and Daniel P. Lowry are supported by Antarctic Science Platform (ANTA1801) and Our Changing Coast (RTVU2206) grants from the New Zealand Ministry of Business, Innovation, and Employment. Torsten Albrecht acknowledge funding by the PalMod project (FKZ: 01LP1925D, 01LP2305B), supported by the German Federal Ministry of Education and Research (BMBF) as a Research for Sustainability initiative (FONA). Violaine Coulon also acknowledges funding by the Fonds de la Recherche Scientifique de Belgique (F.R.S.-FNRS) with an F.R.S.-FNRS Postdoctoral Researcher Fellowship. Javier Blasco acknowledges support by the European Union's Horizon Europe research and innovation programme under grant agreement no. 101137601 (ClimTip). Support for Xylar S. Asay-Davis, Trevor R. Hillebrand and Matthew J. Hoffman was provided through the Scientific Discovery through Advanced Computing (SciDAC) program funded by the US Department of Energy (DOE), Office of Science, Advanced Scientific Computing Research and Biological and Environmental Research Programs. Phillipe Huybrechts and Jonas Van Breedam received support from the Research Foundation Flanders (FWO-Vlaanderen) under project grant no. G091820N. Jonas Van Breedam holds a Junior Postdoctoral Fellowship from the Research Foundation Flanders (FWO-Vlaanderen).

https://doi.org/10.5194/egusphere-2025-4069
Preprint. Discussion started: 14 October 2025

References

Adusumilli, S., Fricker, H. A., Medley, B., Padman, L., and Siegfried, M. R.: Interannual Variations in Meltwater Input to the Southern Ocean from Antarctic Ice Shelves, Nature Geoscience, 13, 616–620, https://doi.org/10.1038/s41561-020-0616-z, 2020.

Arthern, R. J. and Williams, C. R.: The Sensitivity of West Antarctica to the Submarine Melting Feedback, Geophysical Research Letters, 44, 2352–2359, https://doi.org/10.1002/2017GL072514, 2017.

Aschwanden, A. and Brinkerhoff, D. J.: Calibrated Mass Loss Predictions for the Greenland Ice Sheet, Geophysical Research Letters, 49, e2022GL099 058, https://doi.org/10.1029/2022GL099058, 2022.

Aschwanden, A., Bartholomaus, T. C., Brinkerhoff, D. J., and Truffer, M.: Brief Communication: A Roadmap towards Credible Projections of Ice Sheet Contribution to Sea Level, The Cryosphere, 15, 5705–5715, https://doi.org/10.5194/tc-15-5705-2021, 2021.

Barnes, J. M. and Gudmundsson, G. H.: The Predictive Power of Ice Sheet Models and the Regional Sensitivity of Ice Loss to Basal Sliding Parameterisations: A Case Study of Pine Island and Thwaites Glaciers, West Antarctica, The Cryosphere, 16, 4291–4304, https://doi.org/10.5194/tc-16-4291-2022, 2022.

Barthel, A., Agosta, C., Little, C. M., Hattermann, T., Jourdain, N. C., Goelzer, H., Nowicki, S., Seroussi, H., Straneo, F., and Bracegirdle, T. J.: CMIP5 Model Selection for ISMIP6 Ice Sheet Model Forcing: Greenland and Antarctica, The Cryosphere, 14, 855–879, https://doi.org/10.5194/tc-14-855-2020, 2020.

Berdahl, M., Leguy, G., Lipscomb, W. H., and Urban, N. M.: Statistical Emulation of a Perturbed Basal Melt Ensemble of an Ice Sheet Model to Better Quantify Antarctic Sea Level Rise Uncertainties, The Cryosphere, 15, 2683–2699, https://doi.org/10.5194/tc-15-2683-2021, 2021.

Berends, C. J., Stap, L. B., and van de Wal, R. S. W.: Strong Impact of Sub-Shelf Melt Parameterisation on Ice-Sheet Retreat in Idealised and Realistic Antarctic Topography, Journal of Glaciology, 69, 1434–1448, https://doi.org/10.1017/jog.2023.33, 2023.

Brondex, J., Gillet-Chaulet, F., and Gagliardini, O.: Sensitivity of centennial mass loss projections of the Amundsen basin to the friction law, The Cryosphere, 13, 177–195, 2019.

Burgard, C., Jourdain, N. C., Reese, R., Jenkins, A., and Mathiot, P.: An Assessment of Basal Melt Parameterisations for Antarctic Ice Shelves, The Cryosphere, 16, 4931–4975, https://doi.org/10.5194/tc-16-4931-2022, 2022.

Castleman, B. A., Schlegel, N.-J., Caron, L., Larour, E., and Khazendar, A.: Derivation of bedrock topography measurement requirements for the reduction of uncertainty in ice-sheet model projections of Thwaites Glacier, The Cryosphere, 16, 761–778, 2022.

Comeau, D., Asay-Davis, X. S., Begeman, C. B., Hoffman, M. J., Lin, W., Petersen, M. R., Price, S. F., Roberts, A. F., Van Roekel, L. P., Veneziani, M., Wolfe, J. D., Fyke, J. G., Ringler, T. D., and Turner, A. K.: The DOE E3SM v1.2 Cryosphere Configuration: Description and Simulated Antarctic Ice-Shelf Basal Melting, Journal of Advances in Modeling Earth Systems, 14, e2021MS002 468, https://doi.org/10.1029/2021MS002468, 2022.

Cornford, S. L., Seroussi, H., Asay-Davis, X. S., Gudmundsson, G. H., Arthern, R., Borstad, C., Christmann, J., Dias dos Santos, T., Feldmann, J., Goldberg, D., Hoffman, M. J., Humbert, A., Kleiner, T., Leguy, G., Lipscomb, W. H., Merino, N., Durand, G., Morlighem, M., Pollard, D., Rückamp, M., Williams, C. R., and Yu, H.: Results of the third Marine Ice Sheet Model Intercomparison Project (MISMIP+), The Cryosphere, 14, 2283–2301, https://doi.org/10.5194/tc-14-2283-2020, 2020.

Coulon, V., Klose, A. K., Kittel, C., Edwards, T., Turner, F., Winkelmann, R., and Pattyn, F.: Disentangling the Drivers of Future Antarctic Ice Loss with a Historically Calibrated Ice-Sheet Model, The Cryosphere, 18, 653–681, https://doi.org/10.5194/tc-18-653-2024, 2024.

https://doi.org/10.5194/egusphere-2025-4069
Preprint. Discussion started: 14 October 2025

Davison, B. J., Hogg, A. E., Gourmelen, N., Jakob, L., Wuite, J., Nagler, T., Greene, C. A., Andreasen, J., and Engdahl, M. E.: Annual Mass Budget of Antarctic Ice Shelves from 1997 to 2021, Science Advances, 9, eadi0186, https://doi.org/10.1126/sciadv.adi0186, 2023.

De Rydt, J., Jourdain, N. C., Nakayama, Y., van Caspel, M., Timmermann, R., Mathiot, P., Asay-Davis, X. S., Seroussi, H., Dutrieux, P., Galton-Fenzi, B., Holland, D., and Reese, R.: Experimental Design for the Marine Ice Sheet–Ocean Model Intercomparison Project – Phase 2 (MISOMIP2), Geoscientific Model Development, 17, 7105–7139, https://doi.org/10.5194/gmd-17-7105-2024, 2024.

Dutrieux, P., De Rydt, J., Jenkins, A., Holland, P. R., Ha, H. K., Lee, S. H., Steig, E. J., Ding, Q., Abrahamsen, E. P., and Schröder, M.: Strong Sensitivity of Pine Island Ice-Shelf Melting to Climatic Variability, Science, 343, 174–178, https://doi.org/10.1126/science.1244341, 2014.

Edwards, T. L., Nowicki, S., Marzeion, B., Hock, R., Goelzer, H., Seroussi, H., Jourdain, N. C., Slater, D. A., Turner, F. E., Smith, C. J., McKenna, C. M., Simon, E., Abe-Ouchi, A., Gregory, J. M., Larour, E., Lipscomb, W. H., Payne, A. J., Shepherd, A., Agosta, C., Alexander, P., Albrecht, T., Anderson, B., Asay-Davis, X., Aschwanden, A., Barthel, A., Bliss, A., Calov, R., Chambers, C., Champollion, N., Choi, Y., Cullather, R., Cuzzone, J., Dumas, C., Felikson, D., Fettweis, X., Fujita, K., Galton-Fenzi, B. K., Gladstone, R., Golledge, N. R., Greve, R., Hattermann, T., Hoffman, M. J., Humbert, A., Huss, M., Huybrechts, P., Immerzeel, W., Kleiner, T., Kraaijenbrink, P., Le clec'h, S., Lee, V., Leguy, G. R., Little, C. M., Lowry, D. P., Malles, J.-H., Martin, D. F., Maussion, F., Morlighem, M., O'Neill, J. F., Nias, I., Pattyn, F., Pelle, T., Price, S. F., Quiquet, A., Radić, V., Reese, R., Rounce, D. R., Rückamp, M., Sakai, A., Shafer, C., Schlegel, N.-J., Shannon, S., Smith, R. S., Straneo, F., Sun, S., Tarasov, L., Trusel, L. D., Van Breedam, J., van de Wal, R., van den Broeke, M., Winkelmann, R., Zekollari, H., Zhao, C., Zhang, T., and Zwinger, T.: Projected Land Ice Contributions to Twenty-First-Century Sea Level Rise, Nature, 593, 74–82, https://doi.org/10.1038/s41586-021-03302-y, 2021.

Eyring, V., Bony, S., Meehl, G. A., Senior, C. A., Stevens, B., Stouffer, R. J., and Taylor, K. E.: Overview of the Coupled Model Intercomparison Project Phase 6 (CMIP6) Experimental Design and Organization, Geoscientific Model Development, 9, 1937–1958, https://doi.org/10.5194/gmd-9-1937-2016, 2016.

Favier, L., Jourdain, N. C., Jenkins, A., Merino, N., Durand, G., Gagliardini, O., Gillet-Chaulet, F., and Mathiot, P.: Assessment of Sub-Shelf Melting Parameterisations Using the Ocean–Ice-Sheet Coupled Model NEMO(v3.6)–Elmer/Ice(v8.3), Geoscientific Model Development, 12, 2255–2283, https://doi.org/10.5194/gmd-12-2255-2019, 2019.

Fox-Kemper, B., Hewitt, H. T., Xiao, C., Aoalgeirsdottir, G., Drijfhout, S. S., Edwards, T. L., Golledge, N. R., Hemer, M., Kopp, R. E., Krinner, G., Mix, A. C., Notz, D., Nowicki, S., Nurhati, I. S., Ruiz, L., Sallee, J.-B., Slangen, A. B. A., and Yu, Y.: Chapter 9: Ocean, Cryosphere and Sea Level Change, in: Climate Change 2021: The Physical Science Basis. Contribution of Working Group I to the Sixth Assessment Report of the Intergovernmental Panel on Climate Change, edited by Masson-Delmotte, V., Zhai, P., Pirani, A., Connors, S. L., Pean, C., Berger, S., Caud, N., Chen, Y., Goldfarb, L., Gomis, M. I., Huang, M., Leitzell, K., Lonnoy, E., Matthews, J. B. R., Maycock, T., Waterfield, T., Yelekci, O., Yu, R., and Zhou, B., Cambridge University Press, Cambridge, United Kingdom and New York, NY, USA, https://doi.org/10.1017/9781009157896.011, 2021.

Fricker, H. A., Galton-Fenzi, B. K., Walker, C. C., Freer, B. I. D., Padman, L., and DeConto, R.: Antarctica in 2025: Drivers of Deep Uncertainty in Projected Ice Loss, Science, 387, 601–609, https://doi.org/10.1126/science.adt9619, 2025.

Fürst, J. J., Durand, G., Gillet-Chaulet, F., Tavard, L., Rankl, M., Braun, M., and Gagliardini, O.: The Safety Band of Antarctic Ice Shelves, Nature Climate Change, 6, 479–482, https://doi.org/10.1038/nclimate2912, 2016.

Galton-Fenzi, B. K., Porter-Smith, R., Cook, S., Cougnon, E., Gwyther, D. E., Huneke, W. G. C., Rosevear, M. G., Asay-Davis, X., Boeira Dias, F., Dinniman, M. S., Holland, D., Kusahara, K., Naughten, K. A., Nicholls, K. W., Pelletier, C., Richter, O., Seroussi, H. L., and Timmermann, R.: Realistic Ice-Shelf/Ocean State Estimates (RISE) of Antarctic Basal Melting and Drivers, EGUsphere, pp. 1–27, https://doi.org/10.5194/egusphere-2024-4047, 2025.

https://doi.org/10.5194/egusphere-2025-4069
Preprint. Discussion started: 14 October 2025

Garnelo, M., Rosenbaum, D., Maddison, C. J., Ramalho, T., Saxton, D., Shanahan, M., Teh, Y. W., Rezende, D. J., and Eslami, S. M. A.: Conditional Neural Processes, https://doi.org/10.48550/arXiv.1807.01613, 2018.

Gilbert, E. and Kittel, C.: Surface Melt and Runoff on Antarctic Ice Shelves at 1.5°C, 2°C, and 4°C of Future Warming, Geophysical Research Letters, 48, e2020GL091 733, https://doi.org/10.1029/2020GL091733, 2021.

Girden, E. R.: ANOVA: Repeated Measures, SAGE, ISBN 978-0-8039-4257-8, 1992.

Gladstone, R. M., Warner, R. C., Galton-Fenzi, B. K., Gagliardini, O., Zwinger, T., and Greve, R.: Marine Ice Sheet Model Performance Depends on Basal Sliding Physics and Sub-Shelf Melting, The Cryosphere, 11, 319–329, https://doi.org/10.5194/tc-11-319-2017, 2017.

Goldberg, D. N., Gourmelen, N., Kimura, S., Millan, R., and Snow, K.: How Accurately Should We Model Ice Shelf Melt Rates?, Geophysical Research Letters, 46, 189–199, https://doi.org/10.1029/2018GL080383, 2019.

Gwyther, D. E., Cougnon, E. A., Galton-Fenzi, B. K., Roberts, J. L., Hunter, J. R., and Dinniman, M. S.: Modelling the Response of Ice Shelf Basal Melting to Different Ocean Cavity Environmental Regimes, Annals of Glaciology, 57, 131–141, https://doi.org/10.1017/aog.2016.31, 2016.

Hellmer, H. H., Kauker, F., Timmermann, R., Determann, J., and Rae, J.: Twenty-First-Century Warming of a Large Antarctic Ice-Shelf Cavity by a Redirected Coastal Current, Nature, 485, 225–228, https://doi.org/10.1038/nature11064, 2012.

Hill, E. A., Rosier, S. H. R., Gudmundsson, G. H., and Collins, M.: Quantifying the Potential Future Contribution to Global Mean Sea Level from the Filchner–Ronne Basin, Antarctica, The Cryosphere, 15, 4675–4702, https://doi.org/10.5194/tc-15-4675-2021, 2021.

Hoffman, M. J., Asay-Davis, X., Price, S. F., Fyke, J., and Perego, M.: Effect of subshelf melt variability on sea level rise contribution from Thwaites Glacier, Antarctica, Journal of Geophysical Research: Earth Surface, 124, 2798–2822, 2019.

Holland, P. R., Jenkins, A., and Holland, D. M.: The Response of Ice Shelf Basal Melting to Variations in Ocean Temperature, https://doi.org/10.1175/2007JCLI1909.1, 2008.

Jenkins, A.: A One-Dimensional Model of Ice Shelf-Ocean Interaction, Journal of Geophysical Research: Oceans, 96, 20 671–20 677, https://doi.org/10.1029/91JC01842, 1991.

Jenkins, A., Shoosmith, D., Dutrieux, P., Jacobs, S., Kim, T. W., Lee, S. H., Ha, H. K., and Stammerjohn, S.: West Antarctic Ice Sheet Retreat in the Amundsen Sea Driven by Decadal Oceanic Variability, Nature Geoscience, 11, 733–738, https://doi.org/10.1038/s41561-018-0207-4, 2018.

Jordan, J. and the CalvingMIP team: Results from phase one of CalvingMIP, EGU General Assembly 2025, 27 April–2 May 2025, https://doi.org/10.5194/egusphere-egu25-2866, eGU25-2866, 2025.

Joughin, I., Shapero, D., Dutrieux, P., and Smith, B.: Ocean-Induced Melt Volume Directly Paces Ice Loss from Pine Island Glacier, Science Advances, 7, eabi5738, https://doi.org/10.1126/sciadv.abi5738, 2021.

Jourdain, N. C., Asay-Davis, X., Hattermann, T., Straneo, F., Seroussi, H., Little, C. M., and Nowicki, S.: A Protocol for Calculating Basal Melt Rates in the ISMIP6 Antarctic Ice Sheet Projections, The Cryosphere, 14, 3111–3134, https://doi.org/10.5194/tc-14-3111-2020, 2020.

Jourdain, N. C., Mathiot, P., Burgard, C., Caillet, J., and Kittel, C.: Ice shelf basal melt rates in the Amundsen Sea at the end of the 21st century, Geophysical Research Letters, 49, e2022GL100 629, https://doi.org/10.1029/2022GL100629, 2022.

Jourdain, N. C., Amory, C., Kittel, C., and Durand, G.: Changes in Antarctic surface conditions and potential for ice shelf hydrofracturing from 1850 to 2200, The Cryosphere, 19, 1641–1674, https://doi.org/10.5194/tc-19-1641-2025, 2025.

Kachuck, S. B., Whitcomb, M., Bassis, J. N., Martin, D. F., and Price, S. F.: Simulating Ice-Shelf Extent Using Damage Mechanics, Journal of Glaciology, 68, 987–998, https://doi.org/10.1017/jog.2022.12, 2022.

https://doi.org/10.5194/egusphere-2025-4069
Preprint. Discussion started: 14 October 2025

Kruskal, W. H. and Wallis, W. A.: Use of ranks in one-criterion variance analysis, Journal of the American statistical Association, 47, 583–621, 1952.

Lambert, E., Jüling, A., van de Wal, R. S. W., and Holland, P. R.: Modelling Antarctic Ice Shelf Basal Melt Patterns Using the One-Layer Antarctic Model for Dynamical Downscaling of Ice–Ocean Exchanges (LADDIE v1.0), The Cryosphere, 17, 3203–3228, https://doi.org/10.5194/tc-17-3203-2023, 2023.

Lazeroms, W. M. J., Jenkins, A., Gudmundsson, G. H., and van de Wal, R. S. W.: Modelling Present-Day Basal Melt Rates for Antarctic Ice Shelves Using a Parametrization of Buoyant Meltwater Plumes, Cryosphere, 12, 49–70, https://doi.org/10.5194/tc-12-49-2018, 2018.

Leguy, G. R., Lipscomb, W. H., and Asay-Davis, X. S.: Marine Ice Sheet Experiments with the Community Ice Sheet Model, The Cryosphere, 15, 3229–3253, https://doi.org/10.5194/tc-15-3229-2021, 2021.

Levermann, A., Albrecht, T., Winkelmann, R., Martin, M. A., Haseloff, M., and Joughin, I.: Kinematic First-Order Calving Law Implies Potential for Abrupt Ice-Shelf Retreat, Cryosphere, 6, 273–286, 2012.

Levermann, A., Winkelmann, R., Albrecht, T., Goelzer, H., Golledge, N. R., Greve, R., Huybrechts, P., Jordan, J., Leguy, G., Martin, D., Morlighem, M., Pattyn, F., Pollard, D., Quiquet, A., Rodehacke, C., Seroussi, H., Sutter, J., Zhang, T., Van Breedam, J., Calov, R., DeConto, R., Dumas, C., Garbe, J., Gudmundsson, G. H., Hoffman, M. J., Humbert, A., Kleiner, T., Lipscomb, W. H., Meinshausen, M., Ng, E., Nowicki, S. M. J., Perego, M., Price, S. F., Saito, F., Schlegel, N.-J., Sun, S., and van de Wal, R. S. W.: Projecting Antarctica's Contribution to Future Sea Level Rise from Basal Ice Shelf Melt Using Linear Response Functions of 16 Ice Sheet Models (LARMIP-2), Earth System Dynamics, 11, 35–76, https://doi.org/10.5194/esd-11-35-2020, 2020.

Martin, M. A., Winkelmann, R., Haseloff, M., Albrecht, T., Bueler, E., Khroulev, C., and Levermann, A.: The Potsdam Parallel Ice Sheet Model (PISM-PIK) – Part 2: Dynamic Equilibrium Simulation of the Antarctic Ice Sheet, The Cryosphere, 5, 727–740, https://doi.org/10.5194/tc-5-727-2011, 2011.

McCormack, F., Roberts, J., Gwyther, D., Morlighem, M., Pelle, T., and Galton-Fenzi, B.: The impact of variable ocean temperatures on Totten Glacier stability and discharge, Geophysical Research Letters, 48, e2020GL091 790, 2021.

Mirza, M. and Osindero, S.: Conditional Generative Adversarial Nets, https://doi.org/10.48550/arXiv.1411.1784, 2014.

Naughten, K. A., Holland, P. R., Dutrieux, P., Kimura, S., Bett, D. T., and Jenkins, A.: Simulated Twentieth-Century Ocean Warming in the Amundsen Sea, West Antarctica, Geophysical Research Letters, 49, e2021GL094 566, https://doi.org/10.1029/2021GL094566, 2022.

Nowicki, S., Goelzer, H., Seroussi, H., Payne, A. J., Lipscomb, W. H., Abe-Ouchi, A., Agosta, C., Alexander, P., Asay-Davis, X. S., Barthel, A., Bracegirdle, T. J., Cullather, R., Felikson, D., Fettweis, X., Gregory, J. M., Hattermann, T., Jourdain, N. C., Kuipers Munneke, P., Larour, E., Little, C. M., Morlighem, M., Nias, I., Shepherd, A., Simon, E., Slater, D., Smith, R. S., Straneo, F., Trusel, L. D., van den Broeke, M. R., and van de Wal, R.: Experimental protocol for sea level projections from ISMIP6 stand-alone ice sheet models, The Cryosphere, 14, 2331–2368, https://doi.org/10.5194/tc-14-2331-2020, 2020.

Otosaka, I. N., Shepherd, A., Ivins, E. R., Schlegel, N.-J., Amory, C., van den Broeke, M. R., Horwath, M., Joughin, I., King, M. D., Krinner, G., Nowicki, S., Payne, A. J., Rignot, E., Scambos, T., Simon, K. M., Smith, B. E., Sørensen, L. S., Velicogna, I., Whitehouse, P. L., A, G., Agosta, C., Ahlstrøm, A. P., Blazquez, A., Colgan, W., Engdahl, M. E., Fettweis, X., Forsberg, R., Gallée, H., Gardner, A., Gilbert, L., Gourmelen, N., Groh, A., Gunter, B. C., Harig, C., Helm, V., Khan, S. A., Kittel, C., Konrad, H., Langen, P. L., Lecavalier, B. S., Liang, C.-C., Loomis, B. D., McMillan, M., Melini, D., Mernild, S. H., Mottram, R., Mouginot, J., Nilsson, J., Noël, B., Pattle, M. E., Peltier, W. R., Pie, N., Roca, M., Sasgen, I., Save, H. V., Seo, K.-W., Scheuchl, B., Schrama, E. J. O., Schröder, L., Simonsen, S. B., Slater, T., Spada, G., Sutterley, T. C., Vishwakarma, B. D., van Wessem, J. M., Wiese, D., van der Wal, W., and Wouters, B.: Mass Balance of the Greenland and Antarctic Ice Sheets from 1992 to 2020, Earth System Science Data, 15, 1597–1616, https://doi.org/10.5194/essd-15-1597-2023, 2023.

https://doi.org/10.5194/egusphere-2025-4069
Preprint. Discussion started: 14 October 2025

Paolo, F. S., Gardner, A. S., Greene, C. A., Nilsson, J., Schodlok, M. P., Schlegel, N.-J., and Fricker, H. A.: Widespread Slowdown in Thinning Rates of West Antarctic Ice Shelves, The Cryosphere, 17, 3409–3433, https://doi.org/10.5194/tc-17-3409-2023, 2023.

Payne, A. J., Holland, P. R., Shepherd, A. P., Rutt, I. C., Jenkins, A., and Joughin, I.: Numerical Modeling of Ocean-Ice Interactions under Pine Island Bay's Ice Shelf, Journal of Geophysical Research: Oceans, 112, https://doi.org/10.1029/2006JC003733, 2007.

Pelle, T., Morlighem, M., and Bondzio, J. H.: Brief Communication: PICOP, a New Ocean Melt Parameterization under Ice Shelves Combining PICO and a Plume Model, Cryosphere, 13, 1043–1049, https://doi.org/10.5194/tc-13-1043-2019, 2019.

Pollard, D. and DeConto, R. M.: A Simple Inverse Method for the Distribution of Basal Sliding Coefficients under Ice Sheets, Applied to Antarctica, Cryosphere, 6, 953–971, https://doi.org/10.5194/tc-6-953-2012, 2012.

Pollard, D., DeConto, R. M., and Alley, R. B.: Potential Antarctic Ice Sheet Retreat Driven by Hydrofracturing and Ice Cliff Failure, Earth Planet Sci. Lett., 412, 112–121, https://doi.org/10.1016/j.epsl.2014.12.035, 2015.

Ranganathan, M., Robel, A. A., Huth, A., and Duddu, R.: Glacier Damage Evolution over Ice Flow Timescales, EGUsphere, pp. 1–30, https://doi.org/10.5194/egusphere-2024-1850, 2024.

Reese, R., Albrecht, T., Mengel, M., Asay-Davis, X., and Winkelmann, R.: Antarctic Sub-Shelf Melt Rates via PICO, Cryosphere, 12, 1969–1985, https://doi.org/10.5194/tc-12-1969-2018, 2018a.

Reese, R., Gudmundsson, G. H., Levermann, A., and Winkelmann, R.: The Far Reach of Ice-Shelf Thinning in Antarctica, Nature Climate Change, 8, 53–57, https://doi.org/10.1038/s41558-017-0020-x, 2018b.

Reese, R., Garbe, J., Hill, E. A., Urruty, B., Naughten, K. A., Gagliardini, O., Durand, G., Gillet-Chaulet, F., Gudmundsson, G. H., Chandler, D., Langebroek, P. M., and Winkelmann, R.: The Stability of Present-Day Antarctic Grounding Lines – Part 2: Onset of Irreversible Retreat of Amundsen Sea Glaciers under Current Climate on Centennial Timescales Cannot Be Excluded, The Cryosphere, 17, 3761–3783, https://doi.org/10.5194/tc-17-3761-2023, 2023.

Rignot, E. and Jacobs, S. S.: Rapid Bottom Melting Widespread near Antarctic Ice Sheet Grounding Lines, Science, 296, 2020–2023, https://doi.org/10.1126/science.1070942, 2002.

Robel, A. A., Wilson, E., and Seroussi, H.: Layered Seawater Intrusion and Melt under Grounded Ice, The Cryosphere, 16, 451–469, https://doi.org/10.5194/tc-16-451-2022, 2022.

Rosier, S. H. R., Reese, R., Donges, J. F., De Rydt, J., Gudmundsson, G. H., and Winkelmann, R.: The tipping points and early warning indicators for Pine Island Glacier, West Antarctica, The Cryosphere, 15, 1501–1516, https://doi.org/10.5194/tc-15-1501-2021, 2021.

Seroussi, H. and Morlighem, M.: Representation of Basal Melting at the Grounding Line in Ice Flow Models, The Cryosphere, 12, 3085–3096, 2018.

Seroussi, H., Nakayama, Y., Larour, E., Menemenlis, D., Morlighem, M., Rignot, E., and Khazendar, A.: Continued Retreat of Thwaites Glacier, West Antarctica, Controlled by Bed Topography and Ocean Circulation, Geophys. Res. Lett., 44, 6191–6199, https://doi.org/10.1002/2017GL072910, 2017.

Seroussi, H., Nowicki, S., Simon, E., Abe-Ouchi, A., Albrecht, T., Brondex, J., Cornford, S., Dumas, C., Gillet-Chaulet, F., Goelzer, H., Golledge, N. R., Gregory, J. M., Greve, R., Hoffman, M. J., Humbert, A., Huybrechts, P., Kleiner, T., Larour, E., Leguy, G., Lipscomb, W. H., Lowry, D., Mengel, M., Morlighem, M., Pattyn, F., Payne, A. J., Pollard, D., Price, S. F., Quiquet, A., Reerink, T. J., Reese, R., Rodehacke, C. B., Schlegel, N.-J., Shepherd, A., Sun, S., Sutter, J., Van Breedam, J., van de Wal, R. S. W., Winkelmann, R., and Zhang, T.: initMIP-Antarctica: An Ice Sheet Model Initialization Experiment of ISMIP6, The Cryosphere, 13, 1441–1471, https://doi.org/10.5194/tc-13-1441-2019, 2019.

https://doi.org/10.5194/egusphere-2025-4069
Preprint. Discussion started: 14 October 2025

Seroussi, H., Nowicki, S., Payne, A. J., Goelzer, H., Lipscomb, W. H., Abe-Ouchi, A., Agosta, C., Albrecht, T., Asay-Davis, X., Barthel, A., Calov, R., Cullather, R., Dumas, C., Galton-Fenzi, B. K., Gladstone, R., Golledge, N. R., Gregory, J. M., Greve, R., Hattermann, T., Hoffman, M. J., Humbert, A., Huybrechts, P., Jourdain, N. C., Kleiner, T., Larour, E., Leguy, G. R., Lowry, D. P., Little, C. M., Morlighem, M., Pattyn, F., Pelle, T., Price, S. F., Quiquet, A., Reese, R., Schlegel, N.-J., Shepherd, A., Simon, E., Smith, R. S., Straneo, F., Sun, S., Trusel, L. D., Van Breedam, J., van de Wal, R. S. W., Winkelmann, R., Zhao, C., Zhang, T., and Zwinger, T.: ISMIP6 Antarctica: A Multi-Model Ensemble of the Antarctic Ice Sheet Evolution over the 21st Century, The Cryosphere, 14, 3033–3070, https://doi.org/10.5194/tc-14-3033-2020, 2020.

Seroussi, H., Verjans, V., Nowicki, S., Payne, A. J., Goelzer, H., Lipscomb, W. H., Abe-Ouchi, A., Agosta, C., Albrecht, T., Asay-Davis, X., Barthel, A., Calov, R., Cullather, R., Dumas, C., Galton-Fenzi, B. K., Gladstone, R., Golledge, N. R., Gregory, J. M., Greve, R., Hattermann, T., Hoffman, M. J., Humbert, A., Huybrechts, P., Jourdain, N. C., Kleiner, T., Larour, E., Leguy, G. R., Lowry, D. P., Little, C. M., Morlighem, M., Pattyn, F., Pelle, T., Price, S. F., Quiquet, A., Reese, R., Schlegel, N.-J., Shepherd, A., Simon, E., Smith, R. S., Straneo, F., Sun, S., Trusel, L. D., Van Breedam, J., Van Katwyk, P., van de Wal, R. S. W., Winkelmann, R., Zhao, C., Zhang, T., and Zwinger, T.: Insights into the Vulnerability of Antarctic Glaciers from the ISMIP6 Ice Sheet Model Ensemble and Associated Uncertainty, The Cryosphere, 17, 5197–5217, https://doi.org/10.5194/tc-17-5197-2023, 2023.

Seroussi, H., Pelle, T., Lipscomb, W. H., Abe-Ouchi, A., Albrecht, T., Alvarez-Solas, J., Asay-Davis, X., Barre, J.-B., Berends, C. J., Bernales, J., Blasco, J., Caillet, J., Chandler, D. M., Coulon, V., Cullather, R., Dumas, C., Galton-Fenzi, B. K., Garbe, J., Gillet-Chaulet, F., Gladstone, R., Goelzer, H., Golledge, N., Greve, R., Gudmundsson, G. H., Han, H. K., Hillebrand, T. R., Hoffman, M. J., Huybrechts, P., Jourdain, N. C., Klose, A. K., Langebroek, P. M., Leguy, G. R., Lowry, D. P., Mathiot, P., Montoya, M., Morlighem, M., Nowicki, S., Pattyn, F., Payne, A. J., Quiquet, A., Reese, R., Robinson, A., Saraste, L., Simon, E. G., Sun, S., Twarog, J. P., Trusel, L. D., Urruty, B., Van Breedam, J., van de Wal, R. S. W., Wang, Y., Zhao, C., and Zwinger, T.: Evolution of the Antarctic Ice Sheet Over the Next Three Centuries From an ISMIP6 Model Ensemble, Earth's Future, 12, e2024EF004 561, https://doi.org/10.1029/2024EF004561, 2024.

Shepherd, A., Ivins, E., Rignot, E., Smith, B., van den Broeke, M., Velicogna, I., Whitehouse, P., Briggs, K., Joughin, I., Krinner, G., Nowicki, S., Payne, T., Scambos, T., Schlegel, N., A, G., Agosta, C., Ahlstrøm, A., Babonis, G., Barletta, V., Blazquez, A., Bonin, J., Csatho, B., Cullather, R., Felikson, D., Fettweis, X., Forsberg, R., Gallee, H., Gardner, A., Gilbert, L., Groh, A., Gunter, B., Hanna, E., Harig, C., Helm, V., Horvath, A., Horwath, M., Khan, S., Kjeldsen, K. K., Konrad, H., Langen, P., Lecavalier, B., Loomis, B., Luthcke, S., McMillan, M., Melini, D., Mernild, S., Mohajerani, Y., Moore, P., Mouginot, J., Moyano, G., Muir, A., Nagler, T., Nield, G., Nilsson, J., Noel, B., Otosaka, I., Pattle, M. E., Peltier, W. R., Pie, N., Rietbroek, R., Rott, H., Sandberg-Sørensen, L., Sasgen, I., Save, H., Scheuchl, B., Schrama, E., Schröder, L., Seo, K.-W., Simonsen, S., Slater, T., Spada, G., Sutterley, T., Talpe, M., Tarasov, L., van de Berg, W. J., van der Wal, W., van Wessem, M., Vishwakarma, B. D., Wiese, D., Wouters, B., and The IMBIE team: Mass Balance of the Antarctic Ice Sheet from 1992 to 2017, Nature, 558, 219–222, https://doi.org/10.1038/s41586-018-0179-y, 2018.

Taylor, K. E., Stouffer, R. J., and Meehl, G. A.: An Overview of CMIP5 and the Experiment Design, Bulletin of the American Meteorological Society, 93, 485 – 498, https://doi.org/10.1175/BAMS-D-11-00094.1, 2012.

Van Katwyk, P., Fox-Kemper, B., Seroussi, H., Nowicki, S., and Bergen, K. J.: A Variational LSTM Emulator of Sea Level Contribution From the Antarctic Ice Sheet, Journal of Advances in Modeling Earth Systems, 15, e2023MS003 899, https://doi.org/10.1029/2023MS003899, 2023.

von Storch, H. and Zwiers, F. W.: Statistical Analysis in Climate Research, Cambridge University Press, ISBN 978-1-139-42509-4, 2002.

https://doi.org/10.5194/egusphere-2025-4069
Preprint. Discussion started: 14 October 2025

Wang, Y., Zhao, C., Gladstone, R., Zwinger, T., Galton-Fenzi, B. K., and Christoffersen, P.: Sensitivity of the Future Evolution of the Wilkes Subglacial Basin Ice Sheet to Grounding-Line Melt Parameterizations, The Cryosphere, 18, 5117–5137, https://doi.org/10.5194/tc-18-5117-2024, 2024.

Williams, C. R., Thodoroff, P., Arthern, R. J., Byrne, J., Hosking, J. S., Kaiser, M., Lawrence, N. D., and Kazlauskaite, I.: Calculations of Extreme Sea Level Rise Scenarios Are Strongly Dependent on Ice Sheet Model Resolution, Communications Earth & Environment, 6, 1–14, https://doi.org/10.1038/s43247-025-02010-z, 2025.

Wilner, J. A., Morlighem, M., and Cheng, G.: Evaluation of Four Calving Laws for Antarctic Ice Shelves, The Cryosphere, 17, 4889–4901, https://doi.org/10.5194/tc-17-4889-2023, 2023.

Winkelmann, R., Levermann, A., Martin, M. A., and Frieler, K.: Increased Future Ice Discharge from Antarctica Owing to Higher Snowfall, Nature, 492, 239–242, https://doi.org/10.1038/nature11616, 2012.

Zhao, C., Gladstone, R., Galton-Fenzi, B. K., Gwyther, D., and Hattermann, T.: Evaluation of an Emergent Feature of Sub-Shelf Melt Oscillations from an Idealized Coupled Ice Sheet–Ocean Model Using FISOC (v1.1) – ROMSIceShelf (v1.0) – Elmer/Ice (v9.0), Geoscientific Model Development, 15, 5421–5439, https://doi.org/10.5194/gmd-15-5421-2022, 2022.